



All Theses and Dissertations

2007-05-19

Large-Displacement Linear-Motion Compliant Mechanisms

Allen B. Mackay

Brigham Young University - Provo

Follow this and additional works at: <https://scholarsarchive.byu.edu/etd>



Part of the [Mechanical Engineering Commons](#)

BYU ScholarsArchive Citation

Mackay, Allen B., "Large-Displacement Linear-Motion Compliant Mechanisms" (2007). *All Theses and Dissertations*. 901.
<https://scholarsarchive.byu.edu/etd/901>

This Thesis is brought to you for free and open access by BYU ScholarsArchive. It has been accepted for inclusion in All Theses and Dissertations by an authorized administrator of BYU ScholarsArchive. For more information, please contact scholarsarchive@byu.edu, ellen_amatangelo@byu.edu.

LARGE-DISPLACEMENT LINEAR-MOTION
COMPLIANT MECHANISMS

by

Allen Boyd Mackay

A thesis submitted to the faculty of

Brigham Young University

in partial fulfillment of the requirements for the degree of

Master of Science

Department of Mechanical Engineering

Brigham Young University

August 2007

Copyright © 2007 Allen Boyd Mackay

All Rights Reserved

BRIGHAM YOUNG UNIVERSITY

GRADUATE COMMITTEE APPROVAL

of a thesis submitted by

Allen Boyd Mackay

This thesis has been read by each member of the following graduate committee and by majority vote has been found to be satisfactory.

Date

Spencer P. Magleby, Chair

Date

Larry L. Howell

Date

Robert H. Todd

BRIGHAM YOUNG UNIVERSITY

As chair of the candidate's graduate committee, I have read the thesis of Allen Boyd Mackay in its final form and have found that (1) its format, citations, and bibliographical style are consistent and acceptable and fulfill university and department style requirements; (2) its illustrative materials including figures, tables, and charts are in place; and (3) the final manuscript is satisfactory to the graduate committee and is ready for submission to the university library.

Date

Spencer P. Magleby
Chair, Graduate Committee

Accepted for the Department

Matthew R. Jones
Graduate Coordinator

Accepted for the College

Alan R. Parkinson
Dean, Ira A. Fulton College of
Engineering and Technology

ABSTRACT

LARGE-DISPLACEMENT LINEAR-MOTION COMPLIANT MECHANISMS

Allen Boyd Mackay

Department of Mechanical Engineering

Master of Science

Linear-motion compliant mechanisms have generally been developed for small displacement applications. The objective of the thesis is to provide a basis for improved large-displacement linear-motion compliant mechanisms (LLCMs). One of the challenges in developing large-displacement compliant mechanisms is the apparent performance tradeoff between displacement and off-axis stiffness. In order to facilitate the evaluation, comparison, and optimization of the performance of LLCMs, this work formulates and presents a set of metrics that evaluates displacement and off-axis stiffness.

The metrics are non-dimensionalized and consist of the relevant characteristics that describe mechanism displacement, off-axis stiffness, actuation force, and size. Displacement is normalized by the footprint of the device. Transverse stiffness is normalized by a new performance characteristic called virtual axial stiffness. Torsional stiffness is normalized by a performance characteristic called the characteristic torque. Because large-displacement compliant mechanisms are often characterized by non-constant axial and

off-axis stiffnesses, these normalized stiffness metrics are formulated to account for the variation of both axial and off-axis stiffness over the range of displacement.

In pursuit of mechanisms with higher performance, this work also investigates the development of a new compliant mechanism element. It presents a pseudo-rigid-body model (PRBM) for rolling-contact compliant beams (RCC beams), a compliant element used in the RCC suspension. The loading conditions and boundary conditions for RCC beams can be simplified to an equivalent cantilever beam that has the same force-deflection characteristics as the RCC beam. Building on the PRBM for cantilever beams, this paper defines a model for the force-deflection relationship for RCC beams. Included in the definition of the RCC PRBM are the pseudo-rigid-body model parameters that determine the shape of the beam, the length of the corresponding pseudo-rigid-body links and the stiffness of the equivalent torsional spring. The behavior of the RCC beam is parameterized in terms of a single parameter defined as clearance, or the distance between the contact surfaces. The RCC beams exhibit a unique force-displacement curve where the force is inversely proportional to the clearance squared.

The RCC suspension is modeled using the newly defined PRBM. The suspension exhibits unique performance, generating no resistance to axial motion while providing significant off-axis stiffness. The mechanism has a large range of travel and operates with frictionless motion due to the rolling-contact beams. In addition to functioning as a stand-alone linear-motion mechanism, the RCC suspension can be configured with other linear mechanisms in superposition to improve the off-axis stiffness of other mechanisms without affecting their axial resistance.

ACKNOWLEDGMENTS

I wish to express my appreciation to my advisor, Dr. Spencer Magleby, for investing his valuable time in this research. His perspective has helped shape this research, and his encouragement and guidance have been greatly appreciated.

I would also like to thank Dr. Larry Howell, Dr. Robert Todd, and Dr. Brian Jensen for their advice and insights that contributed to my graduate studies and to this work.

I wish to thank my friends and colleagues in the Compliant Mechanisms Research lab. They have provided valuable insights and suggestions that have helped form this work.

I give special thanks to my wife, Jenny, and son, Ethan, for their support and sacrifice. Jenny has expressed constant encouragement and confidence in me throughout this research.

I also express my deep appreciation to my Father in Heaven for the support and inspiration granted to me during the development of this work.

Table of Contents

Acknowledgements	xiii
List of Tables	xvii
List of Figures	xix
1 Introduction	1
1.1 Background and Motivation	1
1.2 Compliant Mechanism Technology	2
1.3 Thesis Objective	3
1.4 Thesis Scope	3
2 Research Approach and Thesis Overview	5
2.1 Thesis outline	6
3 Performance Metrics for Large-Displacement Linear-Motion Mechanisms	7
3.1 Introduction	7
3.2 Literature Review and Background	8
3.2.1 Fundamentals of Force and Stiffness	10
3.2.2 Normalization	13
3.2.3 Key Attributes of LLCMs	13
3.3 Metrics for Large-Displacement Linear Mechanisms	17
3.3.1 Travel Metric	17
3.3.2 Off-Axis Stiffness Metrics	19
3.4 Tailored Metrics for Specific Situations	23
3.5 Demonstration of the Metrics	24
3.6 Conclusions	27
4 Modeling Rolling Contact Compliant Beams with the PRBM	29
4.1 Introduction	29
4.2 Background	30
4.2.1 Review of Cantilever Beam PRBM	32
4.3 Characteristics of RCC Beams	35
4.3.1 Loading Conditions and Boundary Conditions	35
4.3.2 Neutrally-Stable Axial Motion	36
4.4 RCC Beam PRBM Development	37
4.4.1 Derivation of PRBM Parameters	37
4.4.2 Parameterization in Terms of Clearance	39

4.5	PRBM Validation Using FEA	41
4.6	Applying the RCC Beam Model	43
4.7	Example	43
4.8	Conclusions	44
5	Rolling-Contact Compliant Suspension	45
5.1	Introduction and Background	45
5.2	Functional description of the mechanism.	46
5.3	Modeling the RCC Suspension	49
5.4	Superposition and Other Configurations	51
5.5	Procedures used to design the mechanism	53
5.6	Evaluation Using LLCM Metrics	55
5.7	Benefits of the RCC Suspension	55
5.8	Recommendations for future research	56
5.9	Conclusions	57
6	Conclusions	59
	Bibliography	63
	APPENDIX	
A	Simulation of Sample Mechanisms	65
A.1	Folded Beam Simulation	65
A.2	CT Joint Simulation	70
A.3	XBob Simulation	78

List of Tables

3.1	List and description of the key attributes for LLCMs that will be used in the formulation of the performance metrics	16
3.2	Summary of the LLCM Performance Metrics	23
4.1	Pseudo-rigid-body constants for the RCC beam	39
5.1	The dimensions of the RCC suspension in terms of desired displacement . .	54
5.2	Summary of the RCC suspension evaluation	56

List of Figures

3.1	(a) Rigid-body linear roller bearing; (b) Compliant folded-beam mechanism; (c) Compliant bistable mechanism	7
3.2	Conceptual illustration of the performance metrics. The purpose of the metrics is to rate the performance a LLCM design and to facilitate comparison with other designs.	9
3.3	Key definitions for a typical linear-motion compliant mechanism, including axial and transverse directions and total axial displacement	9
3.4	Typical potential energy V , force F , and stiffness k curves for (a) a linear spring, and (b) a bistable mechanism	11
3.5	(a) The ball-on-a-hill analogy uses the mechanism's potential energy curve to illustrate its stability. (b) It can also be used to illustrate the degree of stability by the curvature at a stable point. For example, case F would be considered to be more stable than case G with the ball in the position shown.	12
3.6	The function of transverse stiffness over axial displacement is often non-constant for large-displacement mechanisms, as for this sample folded beam	14
3.7	The function of torsional stiffness over axial displacement is often non-constant for large-displacement mechanisms, as for this sample folded beam	15
3.8	The size of 2D linear mechanisms can be described by the bounding box defined by the widest and longest instances. The limiting features of the support structure indicated by the blue arrows for these three cases.	18
3.9	Illustration of the virtual axial stiffness for (a) a bistable mechanism and (b) linear mechanism	22
3.10	The normalized torsional stiffness can be interpreted as normalized by a characteristic torque as illustrated here with a theoretical mechanism with a force of magnitude $F_{ax,max}$ and couple moment arm of length d	22
3.11	(a) Folded beam [1]; (b) CT joint [2]; (c) XBob [3]	24
3.12	Demonstration of the use of the transverse stiffness metric with several sample configurations.	26
3.13	Demonstration of the use of the torsional stiffness metric with several sample configurations.	26
4.1	Two rolling-contact compliant beams in this application provide spring force against transverse motion	31
4.2	RCC beam illustrating the rolling-contact motion during (a) axial motion and (b) transverse motion	31
4.3	Pseudo-rigid-body model for cantilever beam	33

4.4	(a) Simplification of the boundary conditions and loading conditions to a pinned-pinned segment equivalent to the RCC beam with clearance c , and (b) further simplification to a cantilever beam due to symmetry	36
4.5	Numerical values for α and β for high values of n	38
4.6	Comparison of force-displacement data from the PRBM to FEA	42
4.7	Comparison of stress-displacement data from the PRBM to FEA	42
4.8	Force-displacement relationship for steel beams of thickness 0.075 mm-0.25 mm and yield strengths of 300-1900 MPa.	43
5.1	The RCC suspension uses rolling-contact beams to provide high performance linear travel, illustrated here undergoing (a) axial motion and (b) transverse motion	46
5.2	Closed loop steel RCC beams provide the suspension in this prototype . . .	48
5.3	(a) When subjected to a transverse deflection, resulting forces for the closed-loop configuration are in rotational equilibrium; (b) However, for the open-loop configuration, a transverse deflection causes a resulting moment on the shuttle.	49
5.4	The closed-loop configuration facilitates the implementation of nested RCC beams to multiply the off-axis stiffness. The mechanism illustrated here has $n = 3$ nested beams on each side of the shuttle, resulting in three times the off-axis stiffness.	50
5.5	The clearance on the left and right sides of the shuttle are related by the initial clearance, c_0 , and the transverse deflection, y	51
5.6	The net restoring force, F_{net} due to a transverse displacement, y , from a position on the axis is illustrated here with both beams having an initial clearance c_0	52
5.7	The resulting force deflection curves for the individual RCC beams and the net restoring force for the suspension as functions of off-axis deflection . .	52
5.8	The RCC suspension provides increase stiffness to a mechanism when used in superimposition (x indicates the original mechanism, o indicates the mechanism with the suspension superimposed)	53
5.9	The use of tape springs in the RCC suspension could increase the stiffness because of the stable nature of the two-fold loop	57

Chapter 1

Introduction

Recent maturation in methods for modeling and designing compliant mechanisms has spurred their use in a variety of products, ranging from macro-scale products such as clutches, guides, and switches, to microelectromechanical systems (MEMS). Compliant mechanisms offer a number of advantages, such as increased precision, reduced friction and wear, simple (sometimes monolithic) construction, and reduced assembly. In many ways compliant mechanisms have developed similar functionality to rigid mechanisms. However, compliant mechanisms are faced with their own challenges compared to rigid-body mechanisms that require further development. One particularly elusive aspect of this field is the development of large-displacement linear-motion mechanisms with high off-axis stiffness.

1.1 Background and Motivation

While linear motion is attractive for many applications, mechanisms with large linear displacement generally employ sliding surfaces (prismatic joints) in order to constrain the device to one degree of freedom. Traditional linear-motion mechanisms that use prismatic joints are compact and provide a long range of motion relative to their size. However, prismatic joints have inherent challenges, such as difficulty in lubrication, friction and wear. Due to the clearance in the joint, prismatic joints also often suffer from backlash unless they are manufactured to high tolerances or preloaded. This has led engineers to seek alternatives to prismatic joints for some linear-mechanism applications.

1.2 Compliant Mechanism Technology

Compliant mechanisms could potentially offer an attractive alternative to traditional linear motion mechanisms both in terms of improved functionality and decreased cost. Because compliant mechanisms gain some or all of their motion from deflection of the linkages, they have the potential to completely eliminate relative motion between linkage interfaces (joint surfaces), and thus eliminate friction in the joints. As an added benefit, since compliant members couple energy storage with linkage motion as they deflect, stable positions can be integrated into the design. Several linear motion compliant mechanisms, including bistable mechanisms, have been developed, although they provide much less travel for their size compared to prismatic joints. They are usually employed in mechanisms that require only small displacements, such as micro-relays. Unfortunately, compliant mechanisms that do have a longer travel often have significantly reduced off-axis stiffness due to the use of long flexural members.

Most of the existing linear-motion compliant mechanisms either produce long travel with low off-axis stiffness, or they exhibit high off-axis stiffness over a short range of travel. Also, linear mechanisms have been previously evaluated for off-axis stiffness at a single point, without addressing variations in stiffness throughout their range of travel. This research will focus on developing tools that facilitate the integration of both of these desirable characteristics into the design of future mechanisms. Such large-displacement linear-motion mechanisms (LLCMs) could be applied in products with translating components, such as:

- Handheld electronic devices with translating features
- Media ejectors, such as CD or DVD drives and memory card ejectors
- Retractable devices, such as trays
- Linear positioning devices and kinematic “slider joints” at the MEMS level
- Linear devices in harsh environments where lubrication is not an option

1.3 Thesis Objective

The overall objective of this thesis is to further the development of and ability to design large-displacement linear-motion compliant mechanisms. This will be accomplished through the following sub-objectives: (1) develop an improved approach for evaluating the performance of large-displacement linear-motion compliant mechanisms; and (2) emerging from the principles found in the evaluation method, develop and present a new mechanism configuration that provides increased performance in linear motion, along with an associated design-oriented performance model for the new mechanism.

1.4 Thesis Scope

This study will focus on the performance of linear mechanisms for in-plane motion (rotation and translation in the undesired directions). This 2D approach is extensible to 3D and is a basis for the evaluation of the out-of-plane degrees of freedom. Topics of interest for future study include the extension of these in-plane performance metrics to address resistance to out-of-plane translation and rotation. Future interests also include a comprehensive survey and evaluation of linear-motion mechanisms. Further research in this area may help designers develop principles and guidelines to aid in the development of new and improved LLCMs.

Chapter 2

Research Approach and Thesis Overview

This study begins by providing a way to evaluate existing mechanisms that create linear motion. A number of existing compliant mechanisms will be examined and evaluated in pursuit of understanding the attributes that create large linear displacement. The study will then turn to the development of compliant mechanisms with improved performance. Several desired characteristics will be pursued in the development of these mechanisms, including the following:

First, the mechanism should produce a large displacement relative to the size of the mechanism. The displacement should be evaluated using a normalized metric to take into account the size of the mechanism.

Second, the mechanism should carry a shuttle (the translating component) in one direction, causing no shuttle rotation or off-axis translation. In other words, the mechanism should constrain the shuttle to one degree of freedom. The propensity for a mechanism to resist motion in unwanted directions will be referred to as off-axis stiffness. Mechanisms should provide high off-axis stiffness, which should also be evaluated with a normalized stiffness ratio for each undesired degree of freedom.

A careful evaluation of mechanisms will require the development of appropriate metrics for these characteristics. The metric should describe the performance taking into account the mechanism's behavior throughout its entire range of travel.

These performance metrics will lay the groundwork for the evaluation and improvement of LLCMs by providing a more complete description of a mechanism's performance compared to previous methods. The metrics will lead to principles that help to achieve better performance of LLCMs. The metrics will then be used to demonstrate the improved performance of a new compliant linear-motion device.

2.1 Thesis outline

The main body of this thesis is composed of three main parts, which are presented in Chapters 3, 4, and 5. Chapters 3 and 4 are drawn from articles that were being prepared for publication at the time of the writing of this thesis. As such, they are in a format that can stand alone and independent of the thesis. These chapters provide independent literature reviews and background sections for their respective topics. Only their abstracts and references have been removed and included with those of the rest of the thesis. The information in Chapter 5 was also partially drawn from a paper. The material in it links and builds on the concepts presented in Chapters 3 and 4 and will refer to the background provided in those chapters.

In fulfillment of objective (1), Chapter 3 presents a set of in-plane performance metrics for LLCMs. This chapter reviews the previous work done to characterize off-axis stiffness and extends the current boundary of knowledge by providing a new method for evaluating performance. The new metrics describe travel, transverse stiffness, and torsional stiffness using non-dimensional parameters. This builds a foundation for the evaluation, comparison, and optimization of new large-displacement linear-motion compliant mechanisms.

Objective (2) is addressed in Chapters 4 and 5. A new linear-motion device called the Rolling-Contact Compliant (RCC) suspension is presented in Chapter 5 which performs well according to the new metrics. A design oriented method for the analysis of the suspension is developed by building on the pseudo-rigid-body model method. This model is presented in Chapter 4 to enable its use as a design tool in Chapter 5. The model describes the behavior of the suspension's basic compliant component, the Rolling-Contact Compliant beam, which provides the key features of the mechanism's functionality.

Chapter 3

Performance Metrics for Large-Displacement Linear-Motion Mechanisms

3.1 Introduction

Off axis stiffness, or the propensity for a mechanism to resist motion in unwanted directions, is an important consideration for large-displacement compliant mechanisms [2]. Linear-motion mechanisms generally consist of a support structure that guides a portion of the mechanism, called the shuttle, in linear translation. Several examples are shown in Figure 3.1. Previous studies in linear-motion compliant mechanisms have usually focused on mechanisms with relatively small displacements. These mechanisms have been evaluated using metrics that evaluate performance at a single position, usually the default or “home” position. When considering larger displacements, new metrics and design approaches are needed that account for variability in key performance criteria throughout the entire range of displacement.

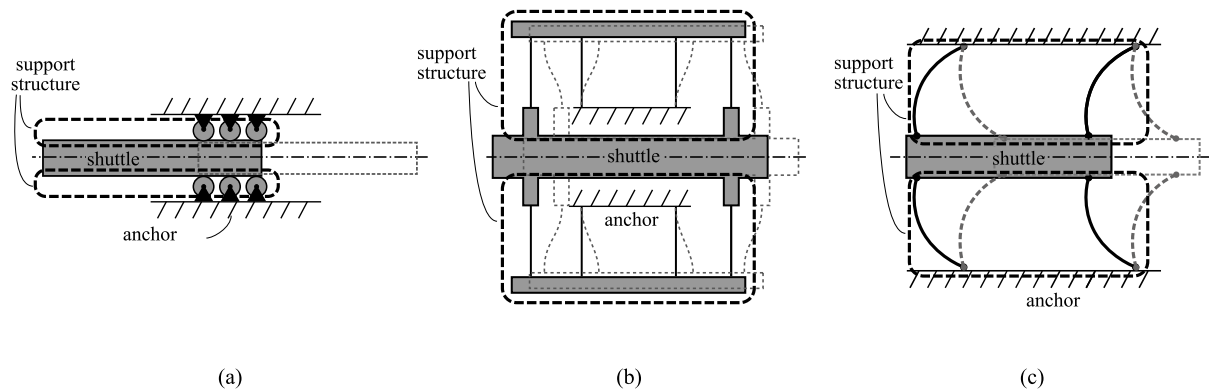


Figure 3.1: (a) Rigid-body linear roller bearing; (b) Compliant folded-beam mechanism; (c) Compliant bistable mechanism

This study seeks to lay the groundwork for the evaluation of large-displacement linear motion compliant mechanisms that approximate the performance of a traditional slider. Optimal mechanism designs should effectively guide the shuttle along the axis of travel, providing resistance to off-axis movement while allowing it to travel relatively freely in the axial direction. The desired outcome of this section is illustrated in Figure 3.2, where performance metrics evaluate the performance for individual designs and also allow comparison between mechanisms. This graphical approach would help to make evident the performance trade-offs due to variations in mechanism design. Several possible candidates for evaluation are illustrated in Figure 3.1. Ideally, the metrics would be capable of evaluating the performance of a wide range of mechanisms, including those with linear force-deflection behavior, as well as those with extremely nonlinear behavior (such as the bistable mechanism shown in Figure 3.1(c)). Note that the metrics developed here do not indicate the overall quality of a mechanism design for every purpose. They are specifically formulated to measure the fitness of a compliant mechanism for large-displacement applications. Many compliant mechanisms have been developed for other purposes and would not be accurately represented by these metrics.

The scope of this work is focused on planar motion. The three aspects of performance that are measured with these metrics include displacement, in-plane transverse stiffness, and in-plane torsional stiffness. Specific applications may call for higher performance in a certain area. Thus it is useful to develop the metrics in a way that makes evident the tradeoffs made when pushing for higher performance. These metrics are developed specifically for application to compliant mechanisms, although the development will draw on rigid-body sliders and theoretical mechanisms in an effort to formulate a robust set of metrics that can evaluate a very large range of mechanism types, including linear mechanisms yet to be developed.

3.2 Literature Review and Background

Several linear motion compliant mechanisms have been developed. Some exhibit nearly linear force-deflection behavior (such as the folded beam [1], the Double V-Beam [4], CT Joint [2], and the XBob [3]), while others exhibit nonlinear, bistable force-deflection

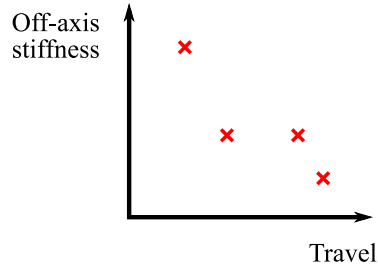


Figure 3.2: Conceptual illustration of the performance metrics. The purpose of the metrics is to rate the performance a LLCM design and to facilitate comparison with other designs.

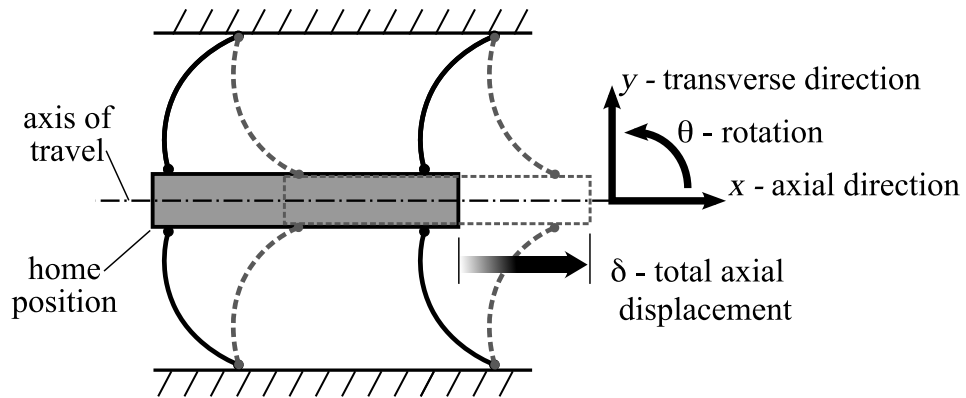


Figure 3.3: Key definitions for a typical linear-motion compliant mechanism, including axial and transverse directions and total axial displacement

behavior (such as the LDBM [5], SRFBM [6], and the DTBM [7]). Travel, δ , and axial and transverse directions are defined for linear-motion mechanisms in Figure 3.3.

With an interest in characterizing the performance of linear mechanisms and in obtaining larger linear displacements, several studies have attempted to address off-axis stiffness properties [1], [2]. Off-axis stiffness has been defined as the ratio of the stiffness in an undesirable direction divided by the stiffness in the intended direction of motion [8]. Several mechanisms in prior work have sought to increase axial displacement while maintaining off-axis stiffness [2]. In these studies, off-axis stiffness has often been evaluated solely based on the resistance to deflection at the as-manufactured or “home” position ($x = 0$). The compliant translational joint developed by Trease et al. [2] exhibited large linear displacement and a high stiffness ratio ($k_{transverse} : k_{axial}$) at the home position. How-

ever, for large displacement mechanisms, the off-axis stiffness must be addressed along the entire range of travel. Off-axis stiffness is usually a function of axial displacement rather than a characteristic of the mechanism [1]. With this in mind, this work will seek to develop a set of performance metrics that accounts for off-axis stiffness across the entire range of axial travel for a given mechanism.

3.2.1 Fundamentals of Force and Stiffness

Keys to the development of a set of off-axis stiffness metrics are a precise definition of stiffness and an understanding of its relationship to force and potential energy. A definition of stiffness can be obtained by examining the relationship that stiffness draws between force and displacement, as

$$F = kx \tag{3.1}$$

Differentiating the equation with respect to x yields

$$\frac{dF}{dx} = k \tag{3.2}$$

Equation (3.2) shows that stiffness, k , corresponds to the slope of a force-displacement curve. Finally, converting the resulting differential terms from (3.2) into finite difference terms results in the following definition for stiffness:

$$k = \frac{\Delta F}{\Delta x} \tag{3.3}$$

In words, equation (3.3) states that stiffness is *the change in force required to take the next step in displacement*. This definition corresponds exactly to the characteristic of interest: we desire mechanisms that will have a quickly increasing restoring force when subjected to a small off-axis displacement, or conversely, that when subjected to an off-axis load, the mechanism displaces a very small amount.

According to this definition, high stiffness is often misused in common vocabulary. To illustrate this, consider a theoretically constant-force mechanism. If the mechanism exhibits a relatively high actuation force, the mechanism could often be incorrectly referred

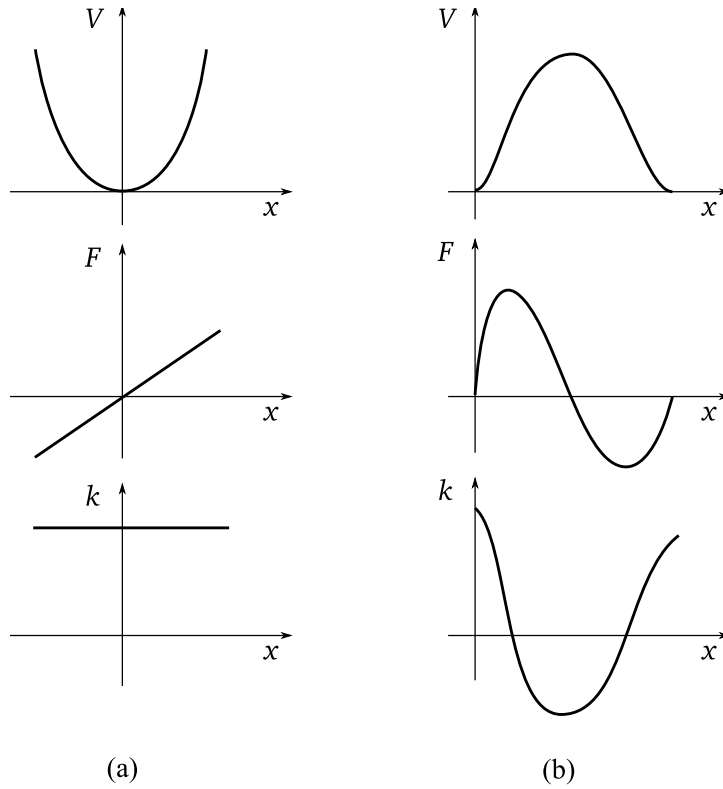


Figure 3.4: Typical potential energy V , force F , and stiffness k curves for (a) a linear spring, and (b) a bistable mechanism

to as “stiff.” However, according to the mathematical definition, a constant force mechanism has zero stiffness. Hence, while stiffness adequately describes the phenomenon of increasing transverse force, it does not describe the actual “feel” of the mechanism, or whether or not the mechanism effectively guides the shuttle along the axis of travel, compared to the force required to actuate the mechanism.

As we seek to find metrics that describe off-axis stiffness, this definition of stiffness and its relationship to force and energy will be important. As equation (3.1) shows, stiffness can be integrated over travel to formulate a function that describes force over displacement. Stiffness can be integrated twice to calculate the potential energy stored in the form of strain energy in a mechanism, as a function of displacement. Figure 3.4 shows typical stiffness, force, and potential energy curves for a linear spring and a bistable mechanism. These curves describe their respective functions along the axial travel.

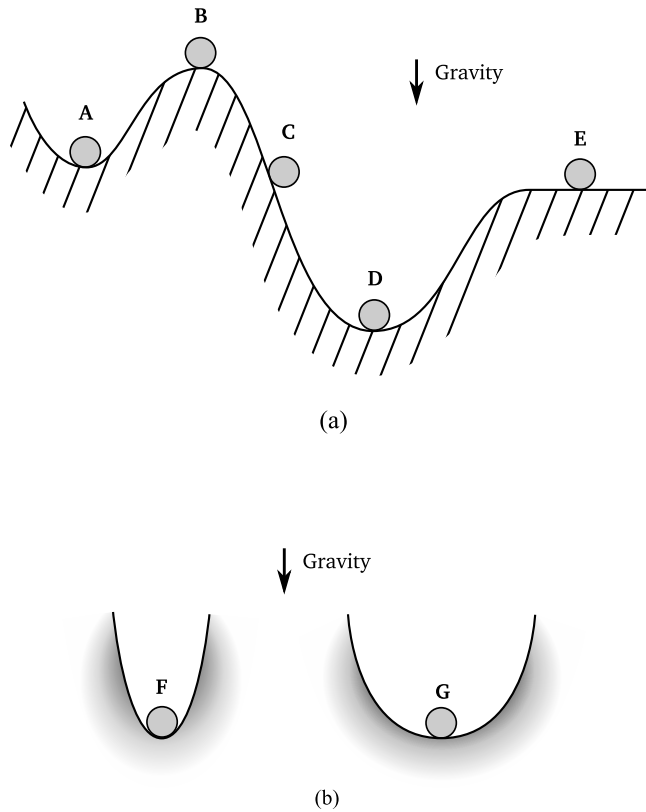


Figure 3.5: (a) The ball-on-a-hill analogy uses the mechanism’s potential energy curve to illustrate its stability. (b) It can also be used to illustrate the degree of stability by the curvature at a stable point. For example, case F would be considered to be more stable than case G with the ball in the position shown.

The potential energy curve, $V(x)$, is often used to visualize stability, or the tendency for a mechanism to return to a position. The ball-on-a-hill analogy in Figure 3.5(a) uses the mechanism’s potential energy curve to illustrate stable points (denoted by local minima in the energy curve) [9]–[11]. The analogy can also illustrate the degree of stability of a mechanism at a stable point by the curvature at that point, as in Figure 3.5(b).

Many linear-motion compliant mechanisms behave like the linear spring in 3.4(a). Examples include the folded beam and the CT joint. These mechanisms can be displaced in both positive and negative x -directions from the home position. From $x = 0$ they can travel forward to $\delta/2$ or back to $-\delta/2$, with a tendency to return to $x = 0$. Bistable mechanisms, in contrast, have a tendency to return to the stable positions at the end of their travel.

They travel from the home position at $x = 0$ to positive δ , the maximum displacement. Depending upon the application, either behavior may be desirable in LLCMs. For either case, however, the axial resistance to motion must be much less than resistance to motion in any off-axis direction.

3.2.2 Normalization

In order to develop a quantitative comparison of mechanism designs and concepts, it will be important to formulate normalized metrics [2]. The creation of non-dimensional metrics allows one to evaluate performance of mechanisms without regard to size. For many linear mechanisms travel can be increased simply by scaling up the size of the mechanism. A proper dimensionless metric for travel would rate scaled versions of the same mechanism as having identical performance. Performance metrics for other characteristics, such as off-axis stiffness, can also be normalized to take into account the scale of the forces involved. This allows one to evaluate, compare, and optimize the inherent form of the mechanism without regard to the size.

Difficulty arises in the case of large displacement compliant mechanisms, where the off-axis stiffness is not always constant, but rather a function of travel (x). A suitable metric would result in a single number representing the critical performance, taking into account the entire range of the mechanism's motion.

3.2.3 Key Attributes of LLCMs

While there are numerous characteristics and functions that describe some aspect of LLCM behavior, only a few have relevance in the evaluation of the performance. This section seeks to elucidate the essential attributes that are relevant and that may be useful in the formulation of metrics.

Two previously mentioned items of interest are the desired off-axis stiffnesses: transverse stiffness, $k_{transv}(x)$, and torsional stiffness, $k_{tors}(x)$. These two important attributes are functions of axial position, as can be seen in Figures 3.6 and 3.7. Because they are often non-constant over the range of travel, it is imperative that representative values be taken from the critical values of the functions rather than relying on a single evaluation

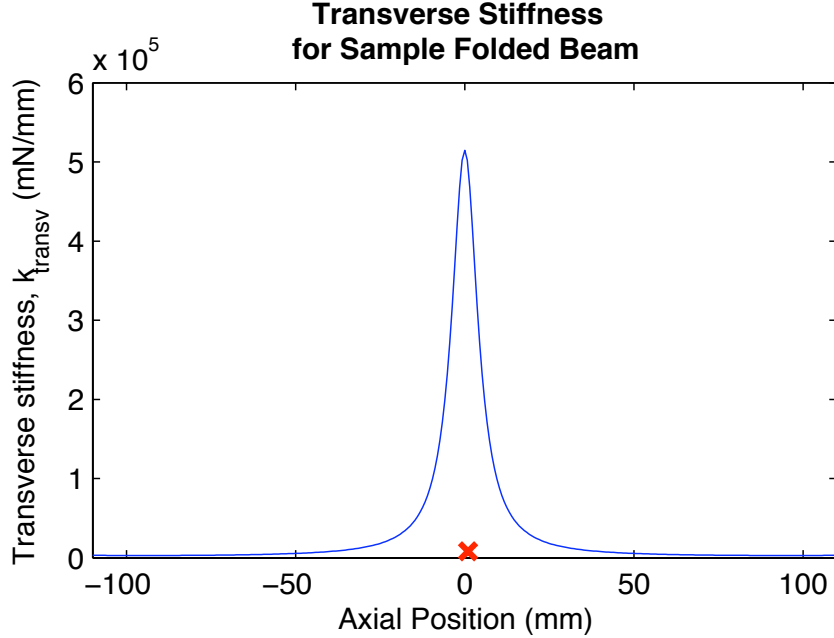


Figure 3.6: The function of transverse stiffness over axial displacement is often non-constant for large-displacement mechanisms, as for this sample folded beam

at the home position. The most critical values for these two functions are the minimum stiffness, $k_{transv,min}$ and $k_{tors,min}$, respectively, whose values are represented by the red x on the respective plots. These functions evaluate transverse and torsional stiffness *on the axis*. The implication of this is that these metrics will assume that stiffness is not a function of y or θ . Since we are interested primarily in the restoring force very near the axis of travel, this assumption does describe the desired performance.

To describe resistance to motion in the desired direction, previous studies often considered the axial stiffness, $k_{ax}(x)$ as a potentially relevant attribute. However, this function has relevance only if the axial stiffness is constant, which is often not the case for large-displacement mechanisms. Stiffness strictly defined is the change in force per change in displacement, or the slope of the force-displacement curve. The large variation in the stiffness of the bistable mechanism in Figure 3.4(b) illustrates a situation where axial stiffness does not describe the overall resistance to deflection.

Axial stiffness is not the resistance one senses when the mechanism is manually actuated. Stiffness is the change in resistance. The outcome of interest in the axial direc-

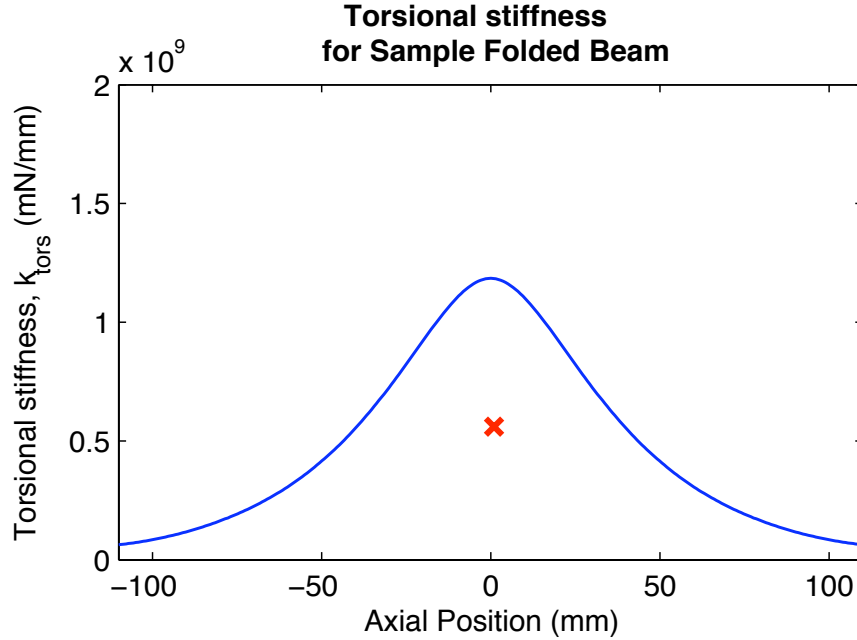
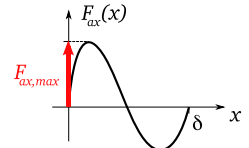
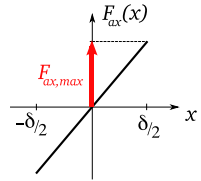
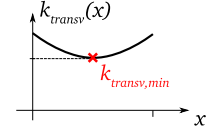
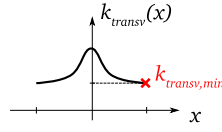
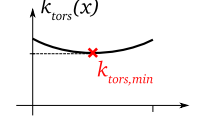
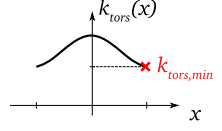
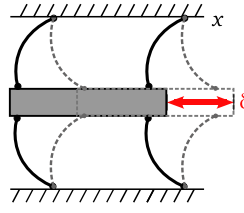
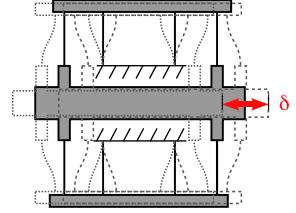
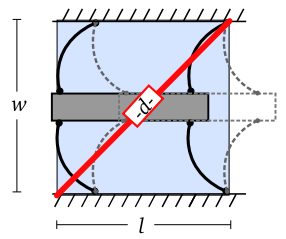
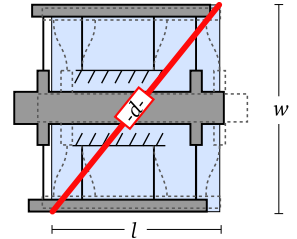


Figure 3.7: The function of torsional stiffness over axial displacement is often non-constant for large-displacement mechanisms, as for this sample folded beam

tion is the *force* required to actuate the mechanism. This is the phenomenon we sense in actuation. Hence, it is the maximum axial force, $F_{ax,max}$, which describes the critical resistance to motion in the axial direction. This actuation force is the maximum axial force over the range of travel. For a mechanism with a linear force-displacement relation, the actuation force corresponds to the force at maximum displacement where $x = \pm\delta/2$, while with a bistable mechanism the actuation force is at an intermediate position. Misdirected actuation forces, which could be the source of transverse loads, are likely to be on the same order of magnitude as the actuation force. Thus this actuation force sets a global scale for the loads associated with the mechanism.

Other key attributes of LLCMs are the total displacement, δ , and the mechanism size, d , defined in Section 3.3.1. The key attributes are listed in Table 3.1. In the following sections, these attributes will be combined to formulate non-dimensional groups that function as suitable performance metrics.

Table 3.1: List and description of the key attributes for LLCMs that will be used in the formulation of the performance metrics

Attribute Description	Critical Value	Variable Name	Bistable Example	Linear Example
Resistance to motion in the desired direction (x)	Maximum axial force	$F_{ax,max}$		
Resistance to motion in the transverse direction (y)	Minimum transverse stiffness	$k_{transv,min}$		
Resistance to rotation (θ)	Minimum torsional stiffness	$k_{tors,min}$		
Total displacement in the desired direction	Displacement	δ		
2-dimensional space requirement	Diagonal of bounding box	d		

3.3 Metrics for Large-Displacement Linear Mechanisms

Compliant mechanisms that would replace traditional sliders need to exhibit large travel with high off-axis stiffness. Performance in these categories is important to overall system performance.

3.3.1 Travel Metric

The ideal LLCM would have large displacement relative to its size. Therefore, a suitable metric for travel would normalize the displacement of a device by its size or footprint. While measuring displacement is straightforward, the definition of the size of a mechanism is a topic to be considered. The discussion that follows seeks to define a characteristic length against which the displacement can be compared. This definition of “mechanism size” will have a large role in normalizing performance in displacement and off-axis stiffness.

Definition of Mechanism Size

Because of packaging considerations, it is often desirable to create the most compact mechanism while delivering the performance needed. For example, handheld devices that incorporate linear motion, such as devices with translating displays or keypads, require mechanisms that deliver large travel while requiring very little “real estate” within the device. Thus the mechanism footprint or size is the maximum space that the mechanism requires during its range of travel. Because this study considers only planar mechanisms, the two-dimensional nature of most linear-motion mechanisms leads us to consider the footprint in the “length” and “width” directions, as indicated in Figure 3.8. These two dimensions create a “bounding box” that encloses the mechanism in its widest and longest instances. The bounding box approach gives preference to compact mechanisms, but it does not limit the application of the metrics to known mechanisms. This opens the possibility of asymmetry or other unique configurations that could be developed in future mechanisms.

The bounding box is defined to include the width and length of the support structure and the portion of the shuttle that contributes to the linear motion, as shown the examples

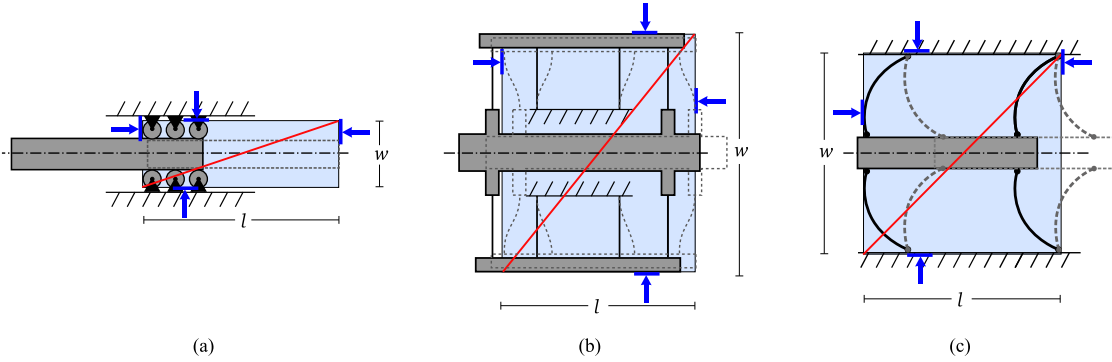


Figure 3.8: The size of 2D linear mechanisms can be described by the bounding box defined by the widest and longest instances. The limiting features of the support structure indicated by the blue arrows for these three cases.

in Figure 3.8. It does not include the anchor or extensions of the shuttle since these features are largely independent of the actual performance of a linear mechanism. The width of the shuttle is included because it is intuitive that torsional stiffness will depend largely upon mechanism size, both in width and length.

These definitions of overall length and width suggest that the optimal size for a mechanism approaches $w = 0$ and $l = \delta$. The ideally sized linear mechanism would have a very narrow support structure, approaching $w = 0$ in the limit. The mechanism's support structure would also be very short (in the axial direction). However, unlike the width, the length of the bounding box does have a non-zero limit, which is set by the length of the shuttle. This ideal can be illustrated with a linear bearing, where the rollers are very small and the mechanism travels the length of the shuttle. This gives the ideally sized mechanism a length of $l = \delta$ in the limit.

Length and width are combined in the normalized displacement metric, δ^* , which uses the length of the diagonal in the bounding box to combine the length and width, as

$$\delta^* = \frac{\delta}{\sqrt{w^2 + l^2}} \quad (3.4)$$

Thus, the length of the diagonal, d , is defined as the characteristic length as

$$d = \sqrt{w^2 + l^2} \quad (3.5)$$

This characteristic length has convenient properties for measuring the mechanism's size. First, the hypotenuse or diagonal of the bounding box is sensitive to changes in both length and width. Second, this combination results in a convenient limit for the size of the ideal mechanism, where the size is equal to displacement ($d = \delta$). When using the hypotenuse to normalize displacement, the resulting travel metric in equation (3.4) has an intuitive lower and upper limit, ranging from the lowest possible performance of 0 to the highest performance of

$$\delta_{max}^* = \frac{\delta}{\delta} = 1 \quad (3.6)$$

Additionally, the hypotenuse provides a metric that is consistent in its ratings, correctly displaying improvements in travel, length, and width.

3.3.2 Off-Axis Stiffness Metrics

The scope of this research will be limited to addressing off-axis stiffness only for in-plane forces, without addressing any out-of-plane moments or out-of-plane forces. The mechanisms will be evaluated for resistance to transverse loads and in-plane torsional loads. These loading conditions simplify the analysis and approximate the majority of off-axis loading conditions for many linear compliant mechanisms, including MEMS (Micro-ElectroMechanical Systems). Future work could extend or modify these metrics to apply to off-axis stiffness in other directions. The discussion that follows outlines the criteria for formulating metrics that could describe off-axis stiffness with a ratio of transverse to axial resistance.

Criteria for Selecting Stiffness Metrics

In the formulation of an off-axis stiffness metric, there are several necessary features that will make the metric effective in evaluating, normalizing, and comparing performance.

- First, the metric must consist of relevant attributes that describe the performance of the mechanism. The key attributes for LLCMs are defined in Section 3.2.3.
- In addition, the metric must consistently rate the performance of all the parameters. In other words, an improvement in any of the components of the metric should result in a better score for the mechanism as a whole. For example, a design change that results in a decrease in axial resistance with all other parameters being held constant should improve the mechanism's score, as should a decrease in size, an increase in displacement, or an increase in off-axis stiffness.
- Finally, the metric should normalize the off-axis stiffness by the undesired axial resistance that is encountered when actuating the mechanism and result in a non-dimensional parameter.

There are several other desirable attributes that, while not necessary, would improve the utility of an off-axis stiffness metric. The metric should be formulated such that it has an intuitive optimum. Perhaps the most intuitive orientation would define the optimum ("high" stiffness) as approaching infinity. The metric should also be able to deal with extremes in off-axis stiffness, such as instabilities in the off-axis direction.

The metric should also capture the relevant information in a way that is simple and meaningful. At times it will be useful for a designer to see a plot of off-axis stiffness over x ($k_{transv}(x)$ or $k_{tors}(x)$). The plot can help the designer visualize the performance of the mechanism over the range of travel and target weaknesses in off-axis stiffness. In this way, the plot performs a similar function to a color plot in stress analysis. A designer may identify areas of low performance in a transverse stiffness plot that actually are irrelevant for specific applications, just as a stress analyst may count as not critical a small area of local yielding in a ductile part. A sample of the off-axis stiffness functions for the folded beam mechanism is shown in Figures 3.6 and 3.7. Note the large change in stiffness as the folded beam is deflected from its home position. In other situations it will be useful to quantify stiffness with a single representative value. This worst case stiffness can be normalized by comparison to the axial resistance. Normalization boils the performance down to a single

non-dimensional number. This single scalar rating is simple enough and contains enough information that it could often be used in numerical optimization programs.

Transverse Stiffness Metric

From the preceding discussion, it can be seen that the items of interest for the transverse and axial resistance are the transverse stiffness, k_{transv} , and the actuation force, $F_{ax,max}$. A simple ratio of these parameters will not result in a dimensionless group. Therefore, one other parameter, the mechanism displacement, δ , is employed to create the normalized transverse stiffness metric, k_{transv}^* , defined as

$$k_{transv}^* = \frac{k_{transv,min}}{F_{ax,max}/\delta} \quad (3.7)$$

This metric successfully integrates the desired qualities of an off-axis stiffness metric as described in Section 3.3.2. It consists entirely of characteristic values. The ratio is unitless, with the denominator resembling an overall stiffness in the axial direction. For this reason it is termed the virtual axial stiffness, $k_{ax,virt}$, where

$$k_{ax,virt} = \frac{F_{ax,max}}{\delta} \quad (3.8)$$

This interpretation of the metric is illustrated in Figure 3.9. For a linear spring with constant stiffness, the virtual stiffness is exactly half the axial stiffness, as in Figure 3.9b.

Torsional Stiffness Metric

Torsional stiffness can be normalized by comparing it to another set of characteristic values, similar to the virtual stiffness. Using a product of mechanism size, d , and the actuation force, the normalized torsional stiffness is defined as

$$k_{tors}^* = \frac{k_{tors,min}}{F_{ax,max} \cdot d} \quad (3.9)$$

This can be interpreted as normalization by a characteristic torque, T_{char} , consisting of a force of magnitude $F_{ax,max}$ and couple moment arm equal to the mechanism size, d , defined

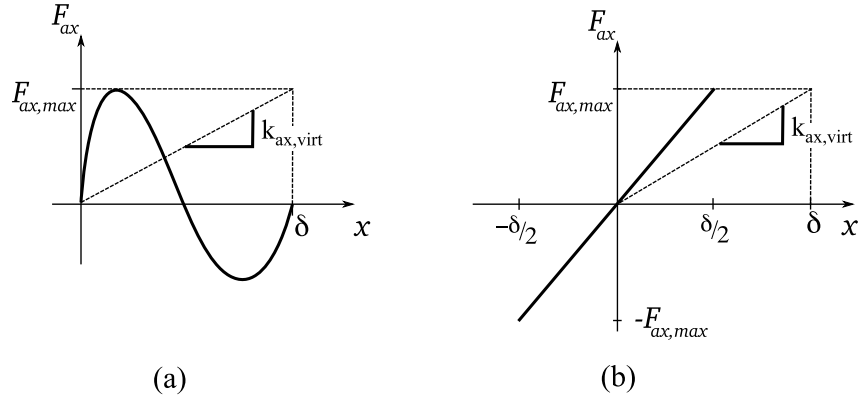


Figure 3.9: Illustration of the virtual axial stiffness for (a) a bistable mechanism and (b) linear mechanism

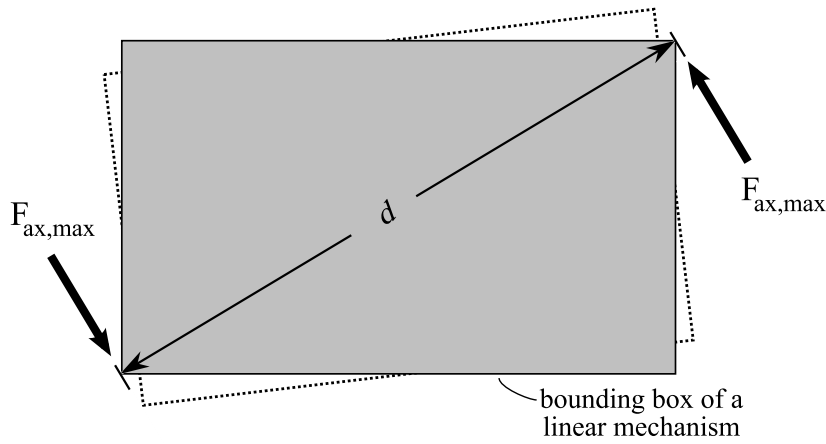


Figure 3.10: The normalized torsional stiffness can be interpreted as normalized by a characteristic torque as illustrated here with a theoretical mechanism with a force of magnitude $F_{ax,max}$ and couple moment arm of length d .

as

$$T_{char} = F_{ax,max} \cdot d \tag{3.10}$$

This interpretation suggests that the metric produces the inverse of the angle (in radians) that results from the application of the characteristic torque. Thus, it is non-dimensional and effectively normalizes the torsional stiffness of the mechanism.

The final form of the travel and stiffness metrics are summarized in Table 3.2

Table 3.2: Summary of the LLCM Performance Metrics

Metric Formula	Normalizing Comparison
$\delta^* = \frac{\delta}{\sqrt{w^2+l^2}}$	Total displacement : device footprint
$k_{transv}^* = \frac{k_{transv,min}}{F_{ax,max}/\delta}$	Minimum transverse stiffness : virtual axial stiffness
$k_{tors}^* = \frac{k_{tors,min}}{F_{ax,max} \cdot d}$	Minimum torsional stiffness : characteristic torque

3.4 Tailored Metrics for Specific Situations

The metrics developed here are formulated to provide the shuttle with highest guidance along the axis of travel. In other words, the metrics reward designs that maximize off-axis stiffness and minimize axial resistance. Special cases may benefit from tailored metrics that describe the objectives for that specific application.

For example, in some applications it is known that the mechanism will be loaded with forces that are significantly higher than the actuation force. This may be especially applicable to cases where the mechanism is neutrally stable (where the mechanism causes no resistance to axial motion). The metrics formulated in 3.3.2 reward these mechanisms with infinite normalized stiffness because they function much like a traditional slider with zero axial resistance. These metrics correctly describe the ratio of off-axis guidance to axial resistance as being extremely high in these cases. However, for two mechanisms with neutrally-stable axial motion, the infinite performance ratings do not allow for comparison of the off-axis stiffness. For practical applications it may be convenient to normalize by the actual scale of forces that the mechanism will encounter. In these cases, it may be convenient to replace the actuation force with an application-specific force, which is termed the maximum operational force, $F_{op,max}$ and would replace the maximum axial force, $F_{ax,max}$ in equation (3.7). The maximum operational force is set by the designer for a specific application and allows the evaluation of mechanisms for that application. This will result in finite performance ratings and allow the comparison of mechanisms with neutrally-stable axial motion.

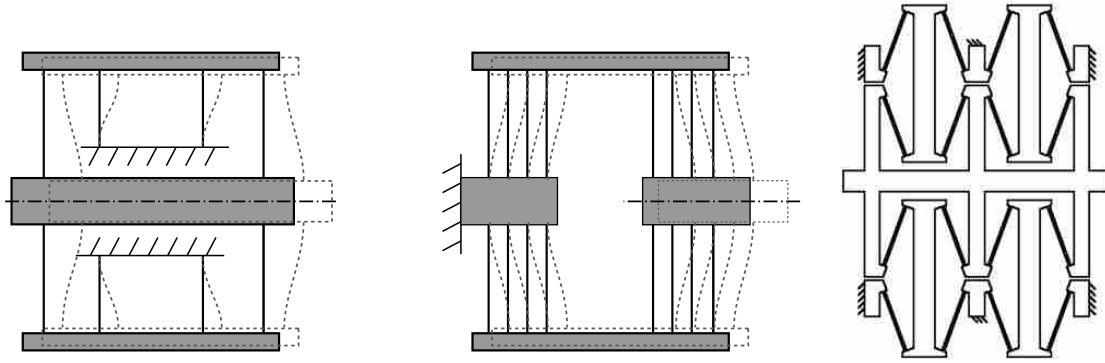


Figure 3.11: (a) Folded beam [1]; (b) CT joint [2]; (c) XBob [3]

3.5 Demonstration of the Metrics

In this section, the performance of a few specific mechanism designs are evaluated to demonstrate the use of the metrics. Several compliant mechanisms were simulated, including the folded beam [1], the CT joint [2], and the XBob [3], pictured in Figure 3.11. The simulations used a commercial finite element analysis capable of nonlinear analysis (ANSYS) with BEAM3 elements. Each simulation represented one of the three basic designs above with a variation in only the in-plane thickness of the flexures, from 1.25-3.0 mm. Details on the simulations and the dimensions of these configurations are included in the appendix. These examples serve to demonstrate the metrics, but they are not a comprehensive evaluation of the potential performance of the devices for all possible configurations.

Performance was evaluated at successive steps along the axis until the maximum stress in a flexure reached the yield strength. Performance for these mechanisms was evaluated using the following procedure:

1. Displace the shuttle axially and record the resulting axial force, $F_{ax}(x)$.
2. Holding the axial position constant, displace the device in the transverse direction (Δy) and record the associated transverse force, $F_{transv}(x)$. Calculate the transverse

stiffness as the transverse force divided by the perturbation, Δy :

$$k_{transv}(x) = \frac{F_{transv}(x)}{\Delta y}. \quad (3.11)$$

3. Continuing to hold the axial position constant, allow the shuttle to return from its transverse displacement, and rotate the shuttle to a small angle ($\Delta\theta$) and record the resulting torque, $T(x)$. Calculate the torsional stiffness as the torque divided by the perturbation angle, $\Delta\Theta$

$$k_{tors}(x) = \frac{T(x)}{\Delta\Theta}. \quad (3.12)$$

4. Determine the total deflection, δ , from physical limitations (e.g. stress limitations or clash of components) or other limits on travel imposed by the designer.
5. Calculate the normalized stiffnesses k_{transv}^* and k_{tors}^* and displacement δ^* using equations (3.4), (3.7), and (3.9). These values determine the performance of one simulation (one of the three mechanisms with a specified flexure thickness), and is represented by a single point on each graph.

The resulting evaluations are shown in Figures 3.12 and 3.13. Each point represents an individual simulation. With more simulations that explore variations in the designs, it could be possible to produce approximate performance regions for each mechanism type (e.g. a cloud of points that describe the folded beam).

Of the designs simulated in this study, the design with the longest travel is a CT joint with very thin flexures. However, this design also has low off-axis stiffness in both the transverse and torsional cases. The Xbob designs possess high transverse stiffness, while the designs of the folded beam exhibit high torsional stiffness. In general, all three concepts show an increase in travel due to the thinning of the flexures.

These examples illustrate the trade-offs made in designing LLCMs. Attempts to increase the off-axis stiffness by increasing the thickness of the flexures results in higher axial resistance. The increase in axial stiffness counteracts the improvement in off-axis stiffness and results in little change in the stiffness ratio. Likewise, attempts to decrease axial resistance through the use of thinner flexures results in lower off-axis stiffness and

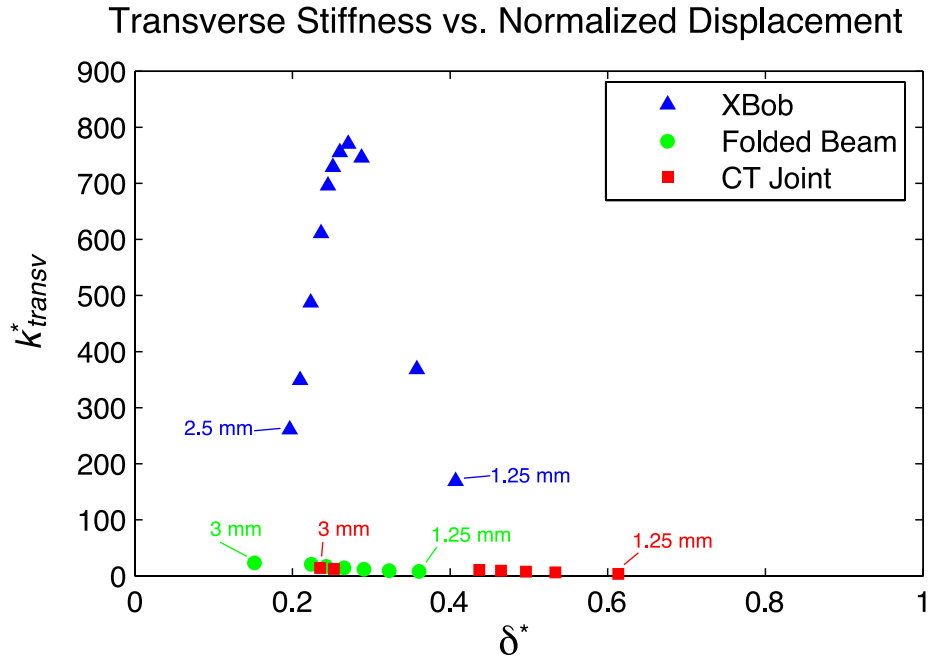


Figure 3.12: Demonstration of the use of the transverse stiffness metric with several sample configurations.

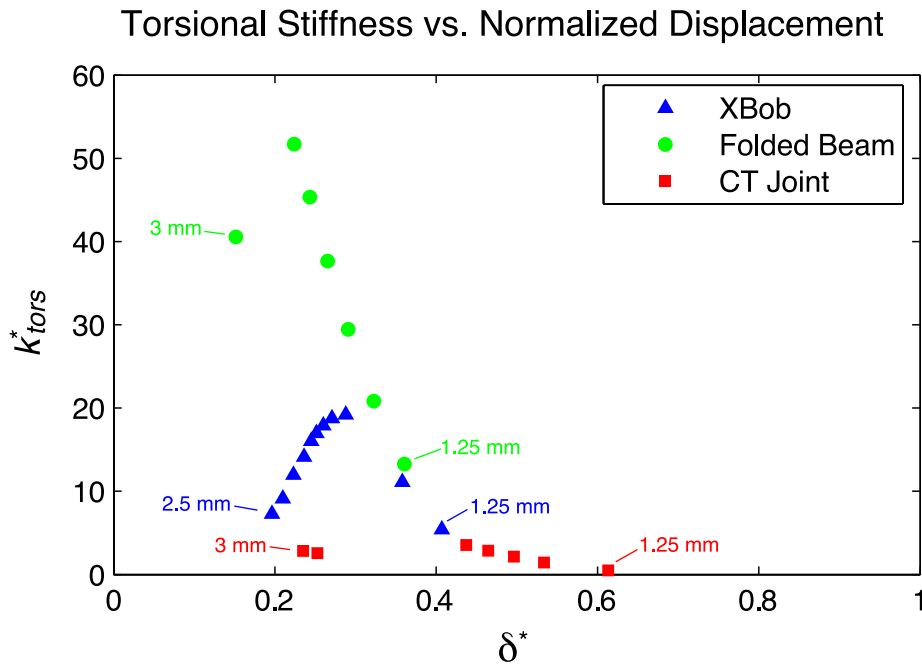


Figure 3.13: Demonstration of the use of the torsional stiffness metric with several sample configurations.

again, little change in the stiffness ratio. It can also be seen that for larger travel, off-axis stiffness generally drops. This suggests that while some small improvements can be made by altering the flexures, there are opportunities at the conceptual level to make significant increases in stiffness. The low off-axis stiffness in many of the designs was due to variation in stiffness. Thus, it would be valuable to have new concepts that obtain consistently high off-axis stiffness.

3.6 Conclusions

This work has developed a foundation for the development and evaluation of new compliant linear mechanisms. These principles may be helpful in developing new devices that overcome the displacement-stiffness trade-offs to yield much longer travel capabilities. The main outcomes of performance for LLCMs are enumerated in the chapter as

1. increased travel
2. increased transverse stiffness
3. increased torsional stiffness
4. decreased axial force
5. decreased mechanism size

These are combined to formulate non-dimensional metrics, which can be used to evaluate mechanism designs. By applying the metrics to designs that span the design space of a concept, the metrics can also compare the performance on a conceptual level.

Chapter 4

Modeling Rolling Contact Compliant Beams with the Pseudo-Rigid-Body Model

As will be shown in Chapter 5, the metrics presented in Chapter 3 indicate that the Rolling-Contact Compliant Beam Suspension has a number of desirable characteristics as a LLCM. This chapter provides a design-oriented model, based on the Pseudo-Rigid-Body Model, that describes the behavior of the suspension's basic element, which is called the Rolling-Contact Compliant (RCC) beam. This investigation of the RCC beam also provides a basis for determining the unique behavior of the RCC suspension.

4.1 Introduction

The pseudo-rigid-body model has enabled designers to successfully predict behavior of many compliant mechanism components. This paper presents a compliant mechanism component called the Rolling-Contact Compliant beam, or RCC beam, and develops and validates a corresponding pseudo-rigid-body model.

The RCC beam consists of a compliant leaf spring that has been elastically deformed into a U-shape, as shown in Figure 4.1. It provides a spring force between two contact surfaces. As the contact surfaces move parallel relative to each other as in Figure 4.2(a), the folded section of the beam rolls along the surface, resulting in smooth, frictionless motion. In addition, because of the constant shape of the rolling contact beam during this axial motion and because all axial positions have the same potential energy, no returning force in the axial direction is generated. However, in the case of transverse motion, where the surfaces move toward each other, the RCC beam acts as a spring to provide a returning force.

In addition to potentially providing frictionless, neutrally-stable axial motion, the rolling-contact motion of the RCC beam exhibits a theoretically infinite range of axial motion, allowing the designer to select any desired axial range of motion [2]. This feature contrasts with typical limited-range linear compliant mechanisms, where the range of travel is usually varied by scaling the entire mechanism.

An analysis tool that effectively predicts the behavior of RCC beams would better enable the use of RCC beams as mechanism components. While several methods could accurately analyze an RCC beam, such as a finite-element analysis model, a faster and more visual method is helpful in iterative design. A design-oriented method can be found in the pseudo-rigid-body model. However, the pseudo-rigid-body model method is limited to the several compliant segment types for which models have been developed (e.g. cantilever beams, pinned-pinned segments, initially-curved cantilever beams [12]–[15]). Models for this mechanism component (the RCC beam) have not previously been developed.

This paper will define RCC beams in greater detail, illustrate some of their unique characteristics, and develop and validate the corresponding pseudo-rigid-body model. The purpose of the model is to aid designers in the analysis of specific beam designs and in design synthesis. With the formulation of the RCC beam pseudo-rigid-body model, designers will be able to quickly synthesize designs that meet their performance specifications. The RCC beam has application in mechanisms that require a spring force. However, this component has the potential to specifically improve performance in linear-motion mechanisms by providing a transverse restoring force throughout a long range of travel (see Figure 4.2(b)).

4.2 Background

The PRBM provides a design-friendly method for analyzing large, nonlinear deflections. By using a simple parametric model for large-deflection compliant segments, it has been shown to reliably predict behavior for many basic compliant mechanisms. Its strength lies in that it decouples the force equations from the deflection equations, allowing them to be solved independently. Because they are parameterized in terms of key parameters, the

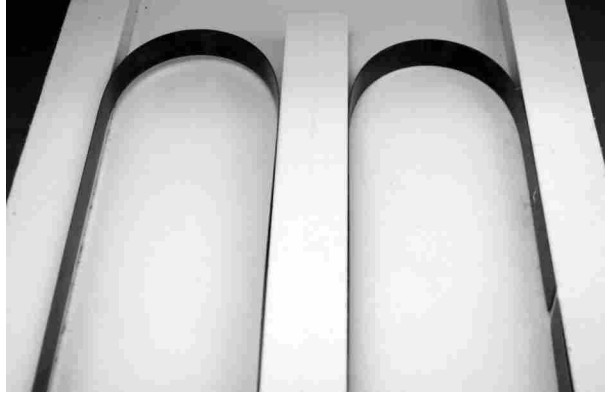


Figure 4.1: Two rolling-contact compliant beams in this application provide spring force against transverse motion

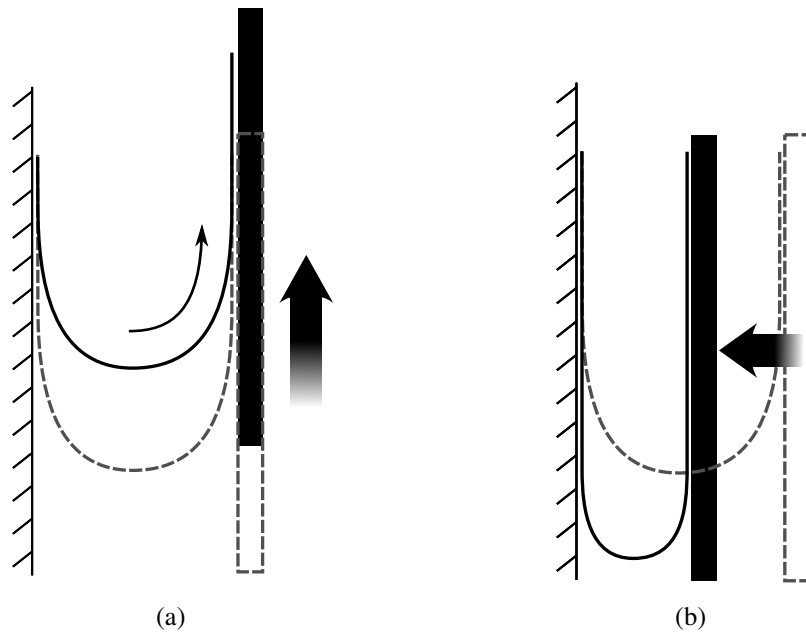


Figure 4.2: RCC beam illustrating the rolling-contact motion during (a) axial motion and (b) transverse motion

model has the ability to quickly predict the behavior of a specific design, and also provides designers with a method for synthesizing a mechanism with the desired behavior.

Pseudo-rigid-body models have been developed to describe the behavior of a number of basic compliant segments [12]–[15]. The cantilever beam model will be a foundation for the development of the pseudo-rigid-body model for RCC beams. Similarities to the pinned-pinned segment model also exist. The approach for simplifying the RCC beams

will be based on the pseudo-rigid-body model for pinned-pinned segments. The following section provides a brief overview of the cantilever beam pseudo-rigid-body model.

The contact-aided nature of the RCC beam builds on previous work in contact-aided compliant mechanisms [16]–[18]. The work on tape springs by Vehar et al. and Seffen involves geometry similar to the RCC beams, employing very long flexible beams [19], [20]. Investigation of the behavior of tape springs in the RCC beam configuration is an interest of future research.

The following sections will show that the boundary conditions for the RCC beam allow the beam to be represented by an equivalent pinned-pinned segment. The PRBM for a pinned-pinned segment exploits symmetry, using a half-model that consists of an initially-curved cantilever beam [13]. The RCC model will follow a similar approach in its use of symmetry. Another applicable principle from previous work in pinned-pinned segments is the determination of the direction of the force applied to these segments. Forces on pinned-pinned segments lie on a line collinear to a line between the pins [15].

Applications of functionally binary pinned-pinned (FBPP) segments include linear displacement bistable mechanisms [21], [22]. RCC beams could apply to similar situations as the FBPP, since the RCC boundary conditions make it essentially a moving pinned-pinned segment. RCC beams may also replace the Rolamite [23] or CORE mechanisms (COMpliant Rolling-contact Element) [18] in applications where the RCC behavior is desirable.

4.2.1 Review of Cantilever Beam PRBM

The PRBM describes the deflection path and force-deflection relationship for a flexible segment by simulating the motion using rigid-body links and torsional springs at the pin joints. For the large-deflection cantilever beam shown in Figure 4.3 the direction of the force at the free end is denoted by the combination of vertical and horizontal force components, P and nP , respectively. The factor n relates to the angle of the force at the beam end, denoted by ϕ , with the resulting force magnitude described as

$$F = P\sqrt{n^2 + 1} \quad (4.1)$$

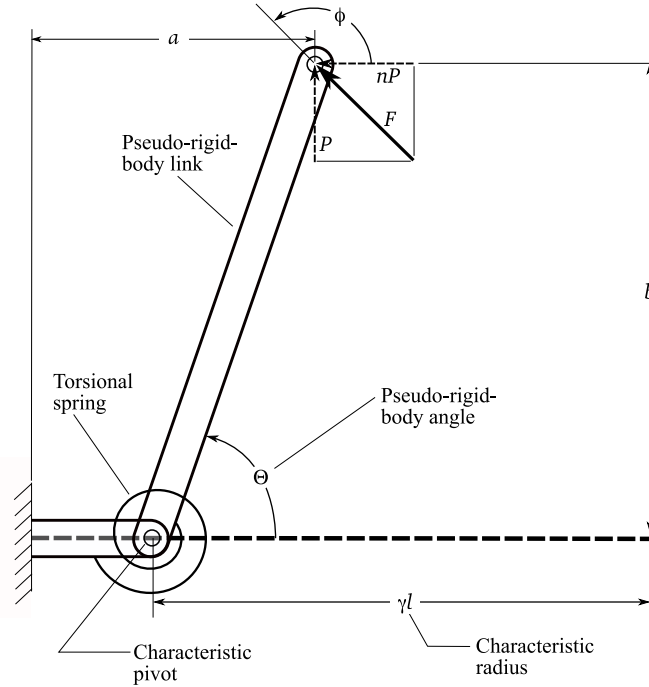


Figure 4.3: Pseudo-rigid-body model for cantilever beam

Predicting the Deflection Path.

To predict the deflection path for large, nonlinear deflections, the pseudo-rigid-body model takes advantage of the nearly circular path that the beam end follows. The cantilever beam deflection path is modeled by two pseudo-rigid-body links, using a characteristic radius factor, γ , to determine the correct ratio of link lengths. For a beam of length l , the radius of the circular deflection path traversed by the pseudo-rigid-body link is the product γl , as illustrated in Figure 4.3. The characteristic radius factor is dependent upon the angle of the force at the free end, which can be determined from the factor n .

Coordinates for the beam end, a and b , are described in terms of the characteristic radius factor, γ , the pseudo-rigid-body angle, Θ , and the length of the cantilever beam, l , as:

$$\frac{a}{l} = 1 - \gamma(1 - \cos(\Theta)) \quad (4.2)$$

and

$$\frac{b}{l} = \gamma \sin(\Theta) \quad (4.3)$$

The highest value of n reported in previous work is for $n = 10$ or $\phi = 174.3^\circ$, where $\gamma = 0.8156$.

Predicting the Force-Deflection Relationship.

The force-deflection relationship is modeled by a torsional spring at the pseudo-rigid-body joint. The value of the torsional spring constant is

$$K = \frac{\gamma K_\Theta EI}{l} \quad (4.4)$$

where K_Θ is the non-dimensional stiffness coefficient, E is the modulus of the material, I is the moment of inertia, and l is the length of the beam. The non-dimensional stiffness coefficient is dependent upon the force angle. For a specified force angle, K_Θ can be found by calculating the tangential load index, $(\alpha^2)_t$, as

$$(\alpha^2)_t = \frac{F_t l^2}{EI} \quad (4.5)$$

and comparing it with the force-deflection relationship for the beam's pseudo-rigid-body link and equivalent torsion spring as

$$(\alpha^2)_t = K_\Theta \Theta \quad (4.6)$$

Equating equations (4.5) and (4.6) and solving for K_Θ yields the non-dimensional stiffness coefficient, K_Θ , for the specified force angle.

A force-deflection relationship can be found by comparing equations for the resulting moment, T , at the pseudo-rigid-body joint (equations (4.7) and (4.8)) and solving for the tangential force at the beam end, F_t .

$$T = K\Theta \quad (4.7)$$

$$T = F_t \gamma l \quad (4.8)$$

4.3 Characteristics of RCC Beams

The RCC beams are leaf springs that have been doubled over to provide a spring force between the two contacting surfaces. As the surfaces move parallel to each other, the folded section of the beam rolls along the surfaces, resulting in smooth, frictionless motion. The RCC beam provides a transverse spring force between the surfaces undergoing anti-parallel motion. This work is limited to mechanisms with straight, parallel contact surfaces and to the region of travel where the beam is in contact with both surfaces.

4.3.1 Loading Conditions and Boundary Conditions

The point of contact where the RCC beam touches the contact surface delineates the curved segment, which spans the gap between the surfaces, and the straight segments, which lie along the contact surface as shown in Figure 4.4(a). Once the beam contacts the surface, the beam is relaxed, lying straight along the surface. Knowing that the bending moment is proportional to curvature, and because this zero-curvature state is identical to the relaxed state of the beam, it can be seen that no moment or distributed load occurs along the straight segment. If there were an applied moment or distributed force, the beam would continue to deflect away from the contacting surface. Therefore, the beam is determined to be point-force loaded at the point of contact. This loading indicates that it is not necessary to analyze the portions of the beam that are in contact with the surfaces, and only the curved portion spanning the gap between the surfaces need be analyzed. The loading on the RCC beam can thus be reduced to an equivalent pinned-pinned segment, with a force applied at the pins and end angles of the segment being parallel to the contact surface.

One notable difference between the basic pinned-pinned segment described by Edwards et al. and the curved segment of the RCC beam shown in Figure 4.4(a) is the initial curvature of the beam. Recalling that in the relaxed state the RCC beam is straight, it can be seen that this equivalent pinned-pinned segment is initially straight, whereas those defined in previous work are circular.

The model of the RCC beam can be simplified by noting that the beam is symmetric across the centerline of the gap between the two contacting surfaces. This symmetry allows

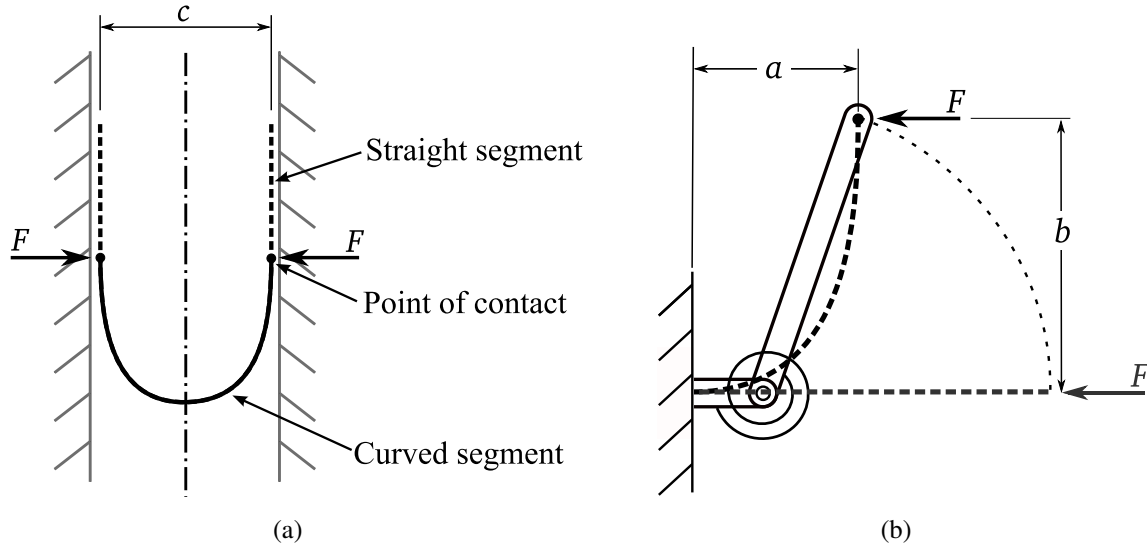


Figure 4.4: (a) Simplification of the boundary conditions and loading conditions to a pinned-pinned segment equivalent to the RCC beam with clearance c , and (b) further simplification to a cantilever beam due to symmetry

the creation and analysis of a half-model of the beam, as illustrated in Figure 4.4(b), where

$$c = 2a \quad (4.9)$$

Thus, the PRBM will use a half-model of the RCC beam, consisting of an initially straight cantilever beam loaded only in the horizontal direction. This equivalent beam is deflected to reach an end angle of 90° . The same set of boundary conditions and loading conditions applies regardless of the distance between contact surfaces. To simulate a narrowing gap between contact surfaces, the length of the equivalent cantilever and corresponding pseudo-rigid-body links also decrease.

4.3.2 Neutrally-Stable Axial Motion

Note that the applied forces on the RCC beam occur along a line collinear to a line between the contact points. In the case of the RCC beam, this results in the force occurring solely in the transverse direction. This important characteristic of RCC beams means that the beam provides transverse spring force but causes no resistance to move the surfaces axially relative to each other.

If the contacting surfaces are straight and parallel, an axial displacement of the surfaces causes the beams to roll along the surfaces without changing the curvature of the beam. As long as the beam is in contact with both surfaces, the radius is constant throughout the axial movement and the energy stored is constant. This constant potential energy area corresponds to a neutrally stable zone. Only when the surfaces undergo transverse motion does the curvature, and thus the reaction force, change.

4.4 RCC Beam PRBM Development

Having simplified the loading conditions of the RCC beam to be equivalent to a cantilever beam with a horizontal load and 90° beam end deflection, the cantilever beam PRBM can be employed.

4.4.1 Derivation of PRBM Parameters

The force angle for the RCC model remains constant. Therefore, the pseudo-rigid-body parameters Θ , γ , and K_{Θ} are constants for any RCC beam. The non-dimensional beam end coordinates, $\frac{a}{l}$ and $\frac{b}{l}$, are also constant for a cantilever with n approaching infinite and end angle of 90°.

Beam End Coordinates.

The coordinates of the beam end, $\frac{a}{l}$ and $\frac{b}{l}$, were obtained using an elliptic integral solution for cantilever beams, recording values of $\frac{a}{l}$ and $\frac{b}{l}$ that correspond to 90.0000° end angles for increasing values of n , up to $n = 525$. Figure 4.5 shows the asymptotic behavior of the coordinates as n increases. Because the RCC beam has an infinite n and a constant end angle of 90°, the non-dimensionalized end coordinates, $\frac{a}{l}$ and $\frac{b}{l}$, will be constants. Two new PRBM constants, α and β , are introduced to define these values as

$$\alpha = \frac{a}{l} = 0.4569 \quad (4.10)$$

and

$$\beta = \frac{b}{l} = 0.7628 \quad (4.11)$$

RCC PRBM Constants: Beam End Coordinates, α and β

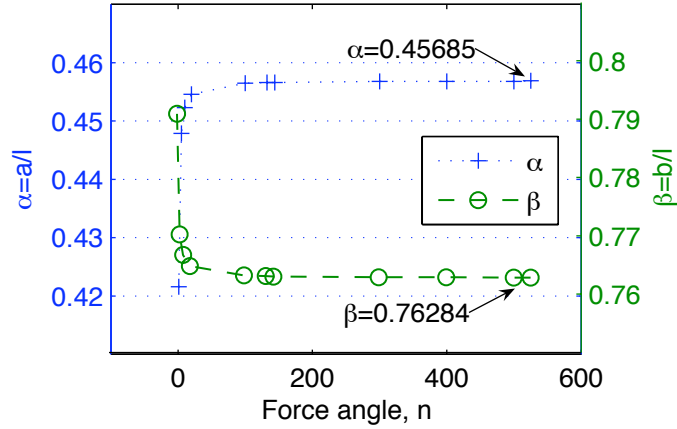


Figure 4.5: Numerical values for α and β for high values of n

Characteristic Radius Factor and Pseudo-Rigid-Body Angle.

Having determined the beam end coordinates, the characteristic radius factor, γ , and the pseudo-rigid-body angle, Θ , can be found by simultaneously solving the beam end equations for a cantilever beam (equations (4.2) and (4.3)). Numerical values for γ and Θ are

$$\Theta = 70.90^\circ \quad (4.12)$$

$$\gamma = 0.8073 \quad (4.13)$$

Torsional Stiffness Coefficient.

As with the cantilever beam PRBM, the torsional stiffness coefficient is found by calculating the non-dimensionalized transverse load index in equations (4.5) and (4.6). This step again uses the output from the elliptical integral solution to determine the equivalent beam's resistance to deflection. For the RCC beam loading configuration, comparing these

Table 4.1: Pseudo-rigid-body constants for the RCC beam

PRBM constant	Value
n	∞
α	0.4569
β	0.7628
γ	0.8073
Θ	70.90°
K_{Θ}	2.625

equations and solving for K_{Θ} results in

$$K_{\Theta} = 2.625 \quad (4.14)$$

4.4.2 Parameterization in Terms of Clearance

The preceding section defines the deflection path and the pseudo rigid body angle for the RCC beam as constants, with the length of the equivalent cantilever beam changing to simulate the narrowing clearance. Perhaps the most useful parameterization for the RCC beams is in terms of the clearance, c , or the distance between the contact surfaces. This section defines the behavior of RCC beams in terms of this parameter.

Dimensions of Cantilever Half-Model.

Because $\frac{a}{l}$ is a constant for an end angle of 90° and very large n , the length of the equivalent cantilever in terms of clearance, $l(c)$, can be modeled using a simple linear relationship as

$$l(c) = \frac{c}{2\alpha} \quad (4.15)$$

The function $b(c)$ can be found with a similar relationship between b and c :

$$b(c) = \frac{\beta c}{2\alpha} \quad (4.16)$$

Pseudo-Rigid-Body Spring Constant.

The pseudo-rigid-body spring constant for a cantilever is given in equation (4.4). For the rolling-contact beam with specified material properties and moment of inertia, all the factors on the right-hand side of equation (4.4) except l are constants defined by (4.13) and (4.14). The spring constant for an RCC beam can be simplified to an inverse relationship with c .

$$K(c) = 2\alpha\gamma K_{\Theta} EI \frac{1}{c} \quad (4.17)$$

$$= 1.936 \frac{EI}{c} \quad (4.18)$$

Force-Deflection Relationship.

Because the force on the equivalent cantilever beam is only in the horizontal direction, the torque at the pseudo-rigid-body spring from equation (4.8) can be rewritten as

$$T = Fb \quad (4.19)$$

and the tangential force from equation (4.8), which is now equal to the total force, can be solved for as

$$F = \frac{K\Theta}{b} \quad (4.20)$$

The force-deflection relationship, $F(c)$, can be found by substituting the equations for the RCC spring stiffness, $K(c)$ and for the end coordinate, $b(c)$, which yields a relationship in terms of clearance, c :

$$F(c) = \frac{4\alpha^2\gamma K_{\Theta}\Theta EI}{\beta} \frac{1}{c^2} \quad (4.21)$$

$$= 2.870 \frac{EI}{c^2} \quad (4.22)$$

Examination of the terms of equation (4.21) shows that the force is inversely proportional to the clearance, c , squared:

$$F(c) \propto \frac{1}{c^2} \quad (4.23)$$

Maximum Stress.

Stress as a function of c can be calculated from bending and axial stress, as follows:

$$\sigma_{max}(c) = \pm \frac{My}{I} - \frac{P}{A} \quad (4.24)$$

$$= \frac{\pm 6Fb}{wh^2} - \frac{F}{wh} \quad (4.25)$$

$$= \frac{F}{wh} \left(\frac{\pm 6\beta c}{2\alpha h} - 1 \right) \quad (4.26)$$

4.5 PRBM Validation Using FEA

Having formulated the pseudo-rigid body model for the RCC beam, a finite element analysis of the beam was created to validate the new model. The finite element model uses a slender, initially-straight beam pinned to two contacting surfaces (one simulating a fixed surface, the other simulating a moving shuttle). While holding one surface fixed, the model steps the shuttle toward the fixed surface until the beam is folded into the rolling-contact configuration. Contact elements between the beam and the two surfaces simulate the contact force, keeping the beam from penetrating the surfaces. The shuttle continues to close the gap between the surfaces, causing the clearance denoted as c to decrease. In addition to the displacement, the model records the resulting force (axial and transverse) and max stress for each step. This validation simulates steel RCC beams ($E = 206.8$ GPa) of rectangular cross-section, with the width $w=10$ mm and the thickness h taking on values of 0.05, 0.10, 0.175, and 0.225 mm. The beams are represented by BEAM3 elements. As can be seen in Figures 4.6 and 4.7, the resulting force-displacement and stress-displacement relationships from the FEA match the PRBM predictions.

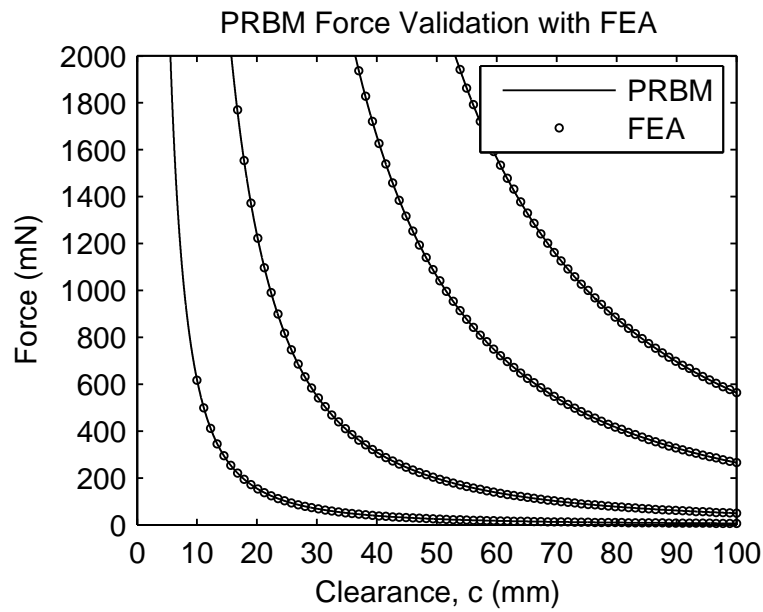


Figure 4.6: Comparison of force-displacement data from the PRBM to FEA

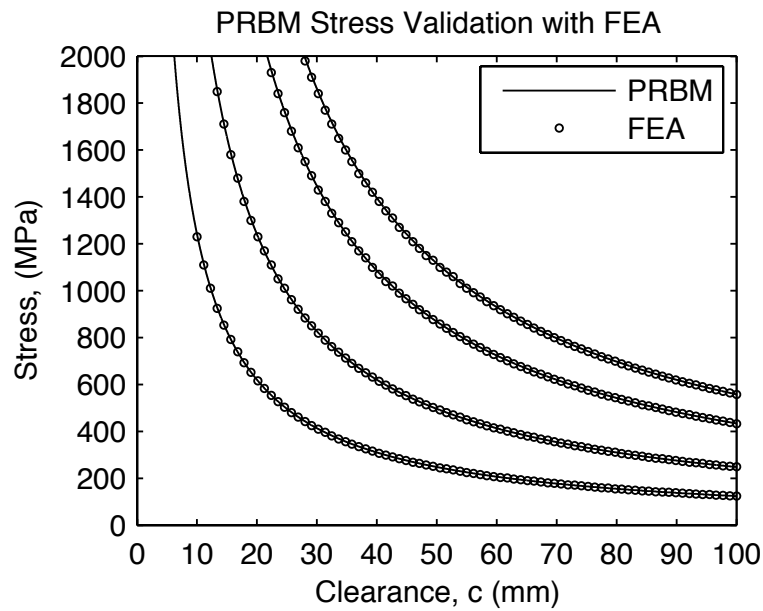


Figure 4.7: Comparison of stress-displacement data from the PRBM to FEA

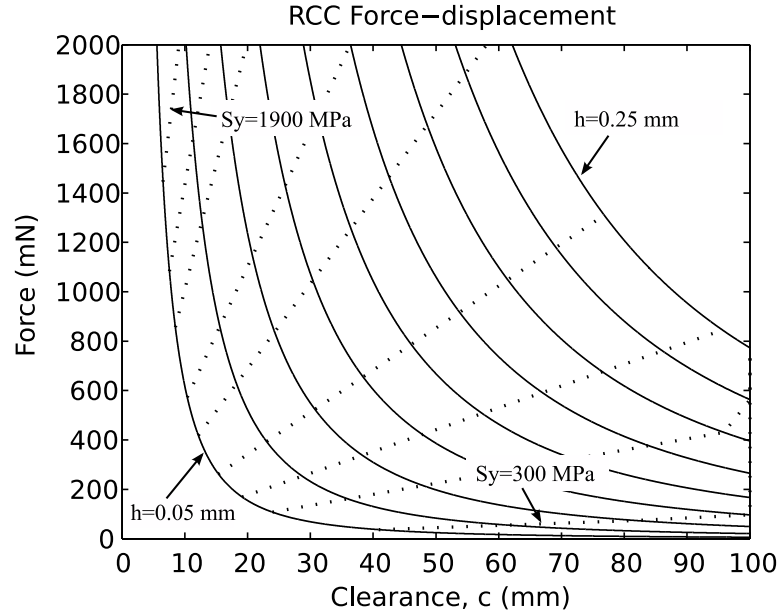


Figure 4.8: Force-displacement relationship for steel beams of thickness 0.075 mm-0.25 mm and yield strengths of 300-1900 MPa.

4.6 Applying the RCC Beam Model

Subsequent studies have shown that RCC beams with large transverse force and narrow clearance are highly preferable. Figure 4.8 shows a sample of the hyperbolic force-deflection curves for steel RCC beams for various stiffness values (thickness, h , ranging from 0.075-0.25 mm (0.003-0.010 in)). Also plotted are the forces at which the beam will yield, depending on the yield strength (S_y ranging from 300-1900 MPa) and indicated by the dotted lines. As the Figure 4.8 illustrates, increasing yield strength quickly improves performance, allowing for higher forces and narrower clearances.

4.7 Example

The PRBM developed above is demonstrated in the following example. Consider an RCC beam made of steel ($E = 206.8$ GPa) of thickness $h = 0.1$ mm and width $w = 10$ mm. Using equation (4.17) the RCC PRBM constants from Table 4.1, the pseudo-rigid-body

spring constant is calculated to be

$$K(c) = \frac{333.7}{c} \text{ N-mm/rad} \quad (4.27)$$

where c is measured in millimeters. Furthermore, the force-deflection relationship is obtained using equation (4.21), resulting in

$$F(c) = \frac{494.5}{c^2} \text{ N} \quad (4.28)$$

Finally, stress is modeled using equation (4.26), resulting in

$$\sigma_{max} = \frac{494.5}{c^2} (50.09c - 1) \text{ MPa} \quad (4.29)$$

$$= \frac{24770}{c} - \frac{494.5}{c^2} \text{ MPa} \quad (4.30)$$

If this beam were deflected to a clearance of $c = 40$ mm, the reaction force would be $F(40) = 0.309$ N with a maximum stress of $\sigma_{max}(40) = 618$ MPa.

4.8 Conclusions

The pseudo-rigid-body model illustrates a number of desirable characteristics for this component. This work has developed a foundation for the development and evaluation of new compliant mechanisms that use this component. Point-force loading at the point of contact allows the RCC beam to be represented by an equivalent pinned-pinned segment, identical to the curved segment of the RCC beam. The PRBM uses a half-model of the RCC beam, consisting of an initially straight cantilever beam loaded only in the horizontal direction. Equations for force and stress are developed in terms of the clearance between contact surfaces. This force-deflection equation is inversely proportional to the clearance squared. Increasing yield strength quickly improves performance, allowing for higher forces and narrower clearances.

Chapter 5

Rolling-Contact Compliant Suspension

Chapter 3 presented a set of in-plane metrics that evaluate the effectiveness of linear motion devices in providing off-axis support across a large range of travel. The metrics developed in that chapter indicate that a high-performance LLCM will have consistently high transverse and torsional stiffness, low axial “actuation” force, large total displacement, and small device footprint. This chapter will present a mechanism that rates highly according to the LLCM metrics, largely due to its extremely low (ideally zero) axial resistance and consistent off-axis stiffness. The mechanism’s basic element, the RCC beam, is described and modeled in Chapter 4. This chapter will provide a functional description of the RCC Suspension. The chapter will also present a model for the RCC suspension using the RCC beam PRBM from Chapter 4, which provides a basis for the associated design procedure.

5.1 Introduction and Background

Recent development in the field of compliant mechanisms has spurred their use in a variety of products, ranging from macro-scale products such as clutches, guides, and switches, to microelectromechanical systems (MEMS). Compliant mechanisms offer a number of advantages over traditional rigid-body mechanisms, such as increased precision, reduced friction and wear, simple (sometimes monolithic) construction, and reduced assembly.

However, compliant mechanisms are faced with their own challenges that require further development. One elusive characteristic in large displacement linear mechanisms is off-axis stiffness. Traditional rigid-body sliders exhibit high off-axis stiffness with small actuation forces (to overcome friction). Linear motion compliant mechanisms that would replace sliding mechanisms must exhibit similar performance in providing high off-axis

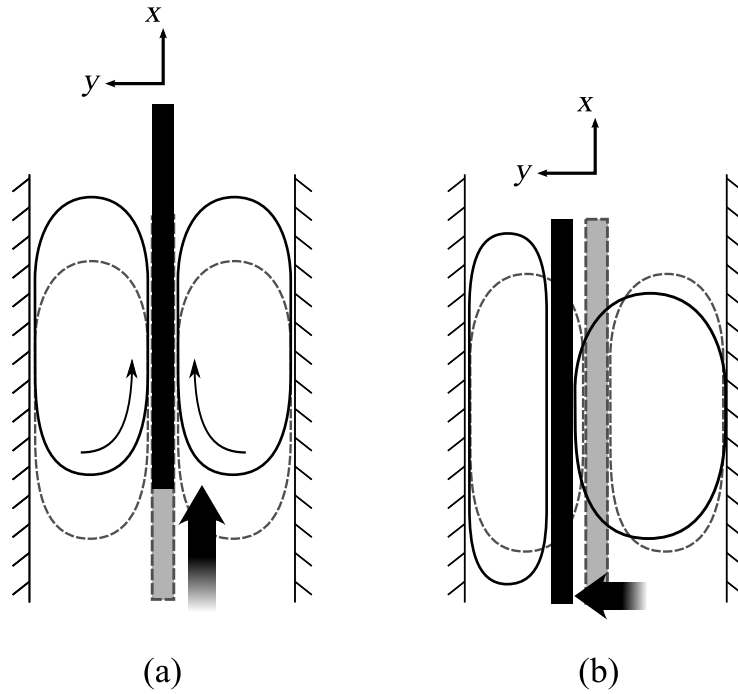


Figure 5.1: The RCC suspension uses rolling-contact beams to provide high performance linear travel, illustrated here undergoing (a) axial motion and (b) transverse motion

stiffness without causing increased resistance in the desired direction of motion. As shown in Chapter 3, for larger displacements, it becomes increasingly important to have consistently high off-axis stiffness. The Rolling Contact Compliant (RCC) suspension, presented in this chapter, functions as a frictionless linear suspension. It provides significant off-axis support while maintaining minimal (ideally zero) resistance to axial motion. Additionally, the device maintains consistent performance at any position throughout the range of travel.

5.2 Functional description of the mechanism.

The RCC suspension is a linear-motion mechanism, formed by symmetric sets of rolling-contact compliant beams, as illustrated in Figure 5.1. RCC beams, described in Chapter 4, consist of flexible leaf springs that have been elastically deformed into a U-shape to provide a spring force between the two contacting surfaces. As the surfaces move parallel to each other, the curved segment of the beams “rolls” along the surfaces, resulting in smooth, frictionless motion.

The RCC suspension configures two or more rolling-contact beams symmetrically across the axis of travel to guide a centrally located shuttle along a linear path, as shown in Figure 5.1(a). These effective spring elements provide continuous lateral support along the length of travel, absorbing transverse loads such as misdirected actuation forces. When a transverse load is applied on the shuttle, the compressed beams create a net force tending to return the shuttle to the axis, as shown in Figure 5.1(b). This transverse stiffness is constant along the entire length of travel, unlike many compliant linear suspension devices (see Section 3.2.3). Because of its unique rolling-contact support beams, the RCC suspension is neutrally stable along its axial travel, and the only input force required is that to overcome inertia and internal losses.

The behavior of the RCC suspension can be seen by examining the behavior of the rolling-contact beams. The straight portion of the beam lying along the surface is relaxed until the point of contact. This lack of curvature evidences that there is no loading on the beam until the point of contact where the curved portion begins. The beam is loaded only at that point of contact, which causes the curved portion of the beam spanning the gap between the surfaces to act as a functionally binary pinned-pinned (FBPP) segment. At any axial position, the beams are symmetric and the points of contact and the forces are mirror images across their centerline. Since forces on FBPP segments act only along the line between the pin joints [15], the resulting forces in the rolling-contact beams is seen to be only in the transverse direction, with no component along the axis of travel. This neutrally-stable axial behavior was also verified with the FEA-based simulation used to validate the PRBM of the rolling-contact beams in Chapter 4. In contrast to the neutrally-stable axial behavior, transverse or rotational deflection of the shuttle causes a returning force due to the change in curvature and in strain energy stored in the beams.

The RCC suspension prototype shown in Figure 5.2 consists of two closed-loop RCC beams. This configuration has several desirable characteristics. Each closed-loop RCC beam conveniently packages two effective RCC beams oriented oppositely on each side of the shuttle. The closed loop creates a suspension point at each end of the shuttle. When the clearance between contact surfaces of an RCC beam decreases, the straight portion of the beam increases in length and the contact points move outward. For the

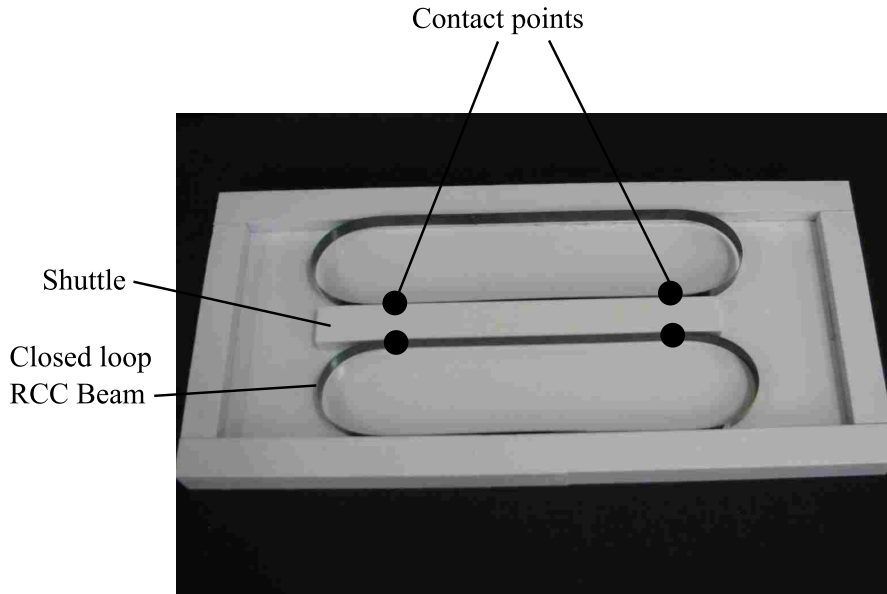


Figure 5.2: Closed loop steel RCC beams provide the suspension in this prototype

closed-loop configuration the points of contact move in the opposite directions along the contact surface when the shuttle displaces transversely, resulting in reaction forces in rotational equilibrium, as shown in Figure 5.3(a). If two individual open-loop RCC beams were oriented in the same direction, replacing the closed-loop RCC beam, the motion of the contact points causes an unbalance in rotation due to the returning forces, as in Figure 5.3. For torsional loads, the movement of the contact points due to rotation of the shuttle actually gives the restoring forces increased moment arms, resulting in increased torsional stability with rotational deflections.

The closed-loop configuration also facilitates implementation of multiple layers of RCC beams in an elegant configuration, as illustrated in Figure 5.4. For many applications, it will be desirable to minimize the space required for the mechanism (largely determined by the clearance). This requires the use very thin RCC beams in order to avoid yielding. However, thinner beams result in much lower returning forces. Higher forces can be achieved using several nested RCC beams. By nesting n beams on each side of the shuttle, the restoring force is multiplied by n (with the associated increase in off-axis stiffness)

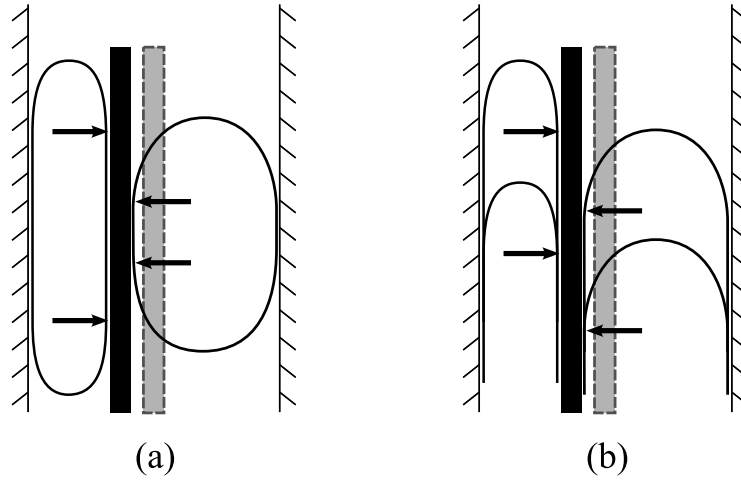


Figure 5.3: (a) When subjected to a transverse deflection, resulting forces for the closed-loop configuration are in rotational equilibrium; (b) However, for the open-loop configuration, a transverse deflection causes a resulting moment on the shuttle.

while causing negligible increase in stress. In the closed-loop configuration the RCC beams operate inside the outer loop.

5.3 Modeling the RCC Suspension

The RCC suspension can be modeled with the pseudo-rigid-body model developed in Chapter 4. The equation for force as a function of clearance between contact surfaces, $F(c)$, from equation (4.21) can be applied at each contact point. The resultant forces are illustrated in Figure 5.6. The net transverse restoring force is the difference in the force from the beams on the left and the right sides of the shuttle. If the beams have identical material properties and geometry, the initial clearance on each side is c_0 , as illustrated in Figure 5.5. The clearances on either side of the shuttle, c_{left} and c_{right} are related by the transverse deflection, y , as

$$c_{left} = c_0 - y \quad (5.1)$$

$$c_{right} = c_0 + y \quad (5.2)$$

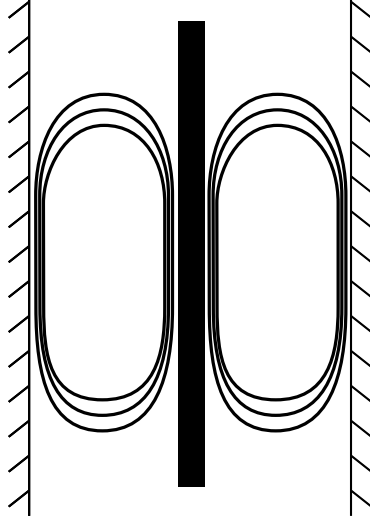


Figure 5.4: The closed-loop configuration facilitates the implementation of nested RCC beams to multiply the off-axis stiffness. The mechanism illustrated here has $n = 3$ nested beams on each side of the shuttle, resulting in three times the off-axis stiffness.

and the net force can be written as a function of transverse deflection, y , as

$$F_{net}(y) = F_{left} - F_{right} \quad (5.3)$$

$$= 2 * 2.870EI \left(\frac{1}{(c_0 - y)^2} - \frac{1}{(c_0 + y)^2} \right) \quad (5.4)$$

Because of the constant shape of the RCC beams, the net force on the shuttle will always tend to restore the shuttle to the axis for a transverse deflection. Because the net force, $F_{net}(y)$, is the same function for any x , the transverse stiffness, $k_{transv}(x)$, also becomes a constant for the mechanism.

$$k_{transv} = \frac{2 * 2.870EI}{y} \left(\frac{n}{(c_0 - y)^2} - \frac{n}{(c_0 + y)^2} \right) \quad (5.5)$$

where c_0 is the initial clearance between contact surfaces, y is the transverse deflection, and n is the number of closed loop beams nested on each side of the shuttle (see Figure 5.4). The maximum stress will occur in the RCC beam being compressed (the left beam for positive y deflection). Thus stress, from equation (4.26), can be rewritten as a function

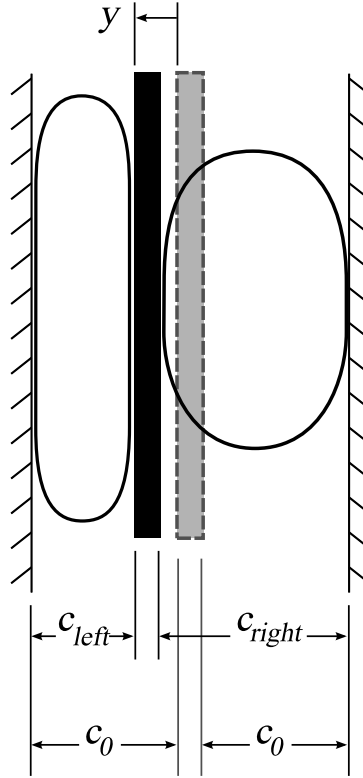


Figure 5.5: The clearance on the left and right sides of the shuttle are related by the initial clearance, c_0 , and the transverse deflection, y .

of transverse deflection as

$$\sigma_{max}(y) = \frac{2.870EI}{wh(c_0)^2} \left(\frac{6\beta(c_0 - y)}{2ah} - 1 \right) \quad (5.6)$$

The behavior of a sample RCC suspension is modeled using the pseudo-rigid-body model in Figure 5.7. The plot shows the resulting force for the individual beams and the net restoring force as functions of transverse deflection, y .

5.4 Superposition and Other Configurations

The RCC suspension can be configured in many ways to fit the needs of specific situations. The planar configuration in Figure 5.1 provides transverse guidance for mechanisms. The suspension could also be employed as a spatial linear mechanism by adding another RCC suspension rotated 90° about the axis of travel.

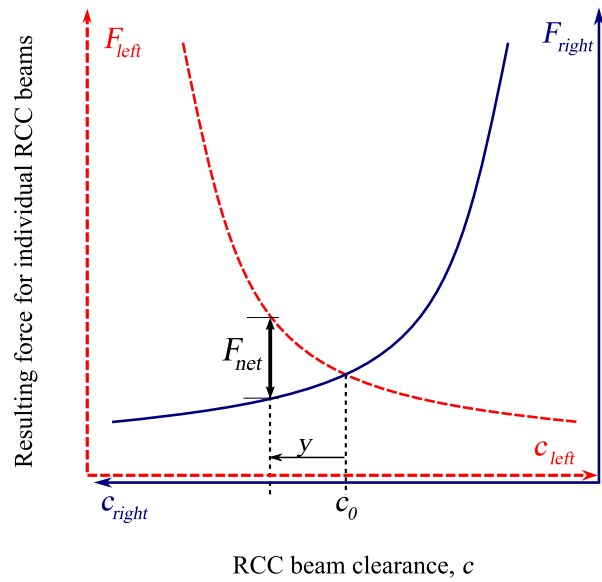


Figure 5.6: The net restoring force, F_{net} due to a transverse displacement, y , from a position on the axis is illustrated here with both beams having an initial clearance c_0 .

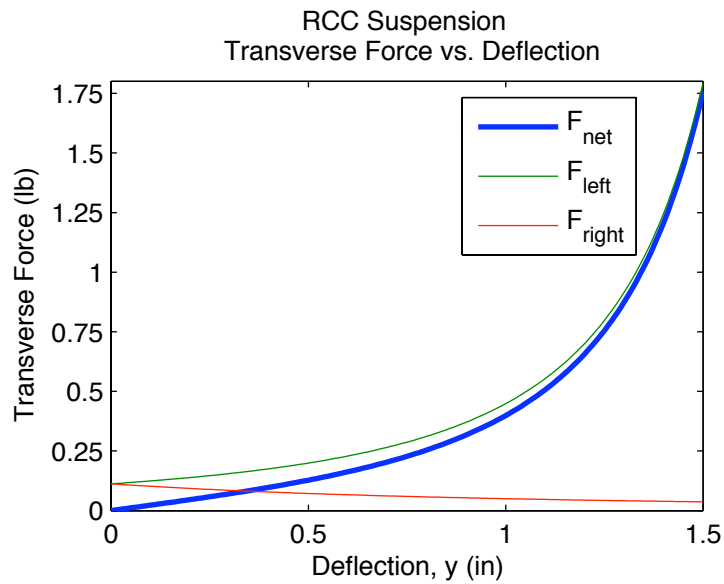


Figure 5.7: The resulting force deflection curves for the individual RCC beams and the net restoring force for the suspension as functions of off-axis deflection

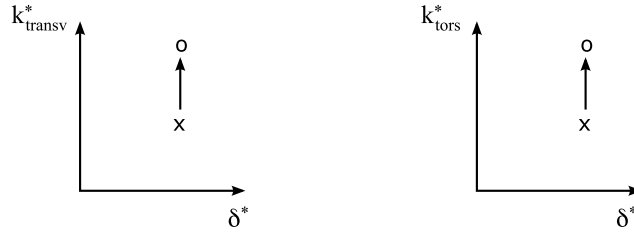


Figure 5.8: The RCC suspension provides increase stiffness to a mechanism when used in superimposition (x indicates the original mechanism, o indicates the mechanism with the suspension superimposed)

As discussed in Chapter 3, one challenge in LLCMs is the effort to increase off-axis stiffness of a mechanism without also affecting the axial resistance. The RCC suspension can help improve the off-axis performance in other linear mechanisms through the principle of superposition. Since the RCC suspension causes no change in axial resistance, the superimposed mechanism's performance directly increases with the additional off-axis stiffness. The resulting performance evaluation is illustrated in Figure 5.8

5.5 Procedures used to design the mechanism

By simultaneously solving the equations for desired force and allowable stress, the designer can generate a set of theoretically feasible designs based on the available beam material thicknesses. These designs all satisfy the force and stress requirements with combinations of the design variables. The designer can then select the most feasible designs based on manufacturability and mechanism size. The design variables are material (yield strength, S_y , and modulus, E), out-of-plane beam thickness (w_{beam}), in-plane beam thickness (t_{beam}) which is generally based on the beam material thickness, the number of nested beams (n), and the initial clearance (c_0), and the maximum off-axis displacement (y_{max}).

In order to maximize the off-axis stiffness, it is desirable to optimize the initial clearance so the force-displacement slope is the highest (the force changes quickly), without causing the beam material to yield. Therefore, it will be advantageous to set the clearance so that the maximum desired restoring force occurs just before the point of yielding.

Table 5.1: The dimensions of the RCC suspension in terms of desired displacement

Dimension	Required Magnitude
$l_{shuttle}$	$2\delta + \frac{y_{max}}{\alpha}$
$l_{contactsurface}$	$2\delta + \frac{y_{max}}{\alpha}$
$w_{overall}$	$2c_0 + w_{shuttle}$
$l_{overall}$	$3\delta + \frac{y_{max}}{\alpha}$

The critical dimensions for this design of the RCC suspension pictured in Figure 5.1 are based on the desired travel, δ and the initial clearance, c_0 . The designer can specify any desired displacement from which necessary dimensions can be calculated. A relationship for the required dimensions can first be formulated for the mechanism at the axial position (where $y = 0$). For a position on the axis, the required length of the shuttle and of the contact surfaces is equal to twice the displacement. The width of the entire support structure is $2c_0 + w_{shuttle}$. Since all the contact surfaces are included in the support structure, the maximum length of the entire structure at any instance is 3δ . A small amount of additional length will be required to allow for contact points to extend along the contact surfaces, depending on the maximum transverse displacement, y_{max} . From equation (4.15), the needed increase in length for the shuttle and contact surfaces due to the motion of the contact points is equal to the change in length of the curved segment at each end, as

$$\Delta l_{max} = 2(l_0 - l_{left}) \quad (5.7)$$

$$= 2 \left(\frac{c_0}{2\alpha} - \frac{(c_0 - y)}{2\alpha} \right) \quad (5.8)$$

$$= \frac{y_{max}}{\alpha} \quad (5.9)$$

Table 5.1 summarizes the dimensions of the RCC suspension as functions of the desired displacement.

5.6 Evaluation Using LLCM Metrics

The LLCM performance metrics developed in Chapter 3 can be used to evaluate the RCC suspension. The overall length, width, and travel in Table 5.1 can be used to evaluate normalized displacement, defined in equation (3.4), which results in

$$\delta^* = \frac{\delta}{\sqrt{(2c_0 + w_{shuttle})^2 + (3\delta + \frac{y_{max}}{\alpha})^2}} \quad (5.10)$$

For mechanisms where the displacement is much larger than the width, the normalized displacement becomes approximately

$$\delta^* \approx \frac{1}{3} \quad (5.11)$$

The off-axis stiffnesses are evaluated using equations (3.7), yielding

$$k_{transv}^* = \infty \quad (5.12)$$

and

$$k_{tors}^* = \infty \quad (5.13)$$

because $F_{ax,max}$ is zero for the RCC suspension. This ratio shows that the suspension successfully imitates the function of a kinematic slider, with its transverse stiffness greatly exceeding the axial resistance. These results are summarized in Table 5.2. For more practical purposes in design, it may be desirable to evaluate the mechanism for specific loading situations. In this case, the mechanism is evaluated by comparing the off-axis stiffness to the operational force, as discussed in Section 3.4. This will yield a finite stiffness value, depending on the operational force specified by the designer.

5.7 Benefits of the RCC Suspension

Applications of the RCC suspension could include products with translating components, such as handheld electronic devices with translating features (e.g. sliding displays or keypads); media ejectors, such as CD or DVD drives and memory card ejectors; re-

Table 5.2: Summary of the RCC suspension evaluation

Metric	Magnitude
δ^*	≈ 0.33
k_{transv}^*	∞
k_{tors}^*	∞

tractable devices, such as trays; linear positioning devices, such as on the MEMS level, including devices that would require kinematic sliders in MEMS; and linear devices in harsh environments where lubrication is not an option.

The manufacturability of the mechanism relies on the designer’s choice of material and thickness for the RCC beams. Materials with a high modulus and high strength-to-modulus ratio will allow for more compact mechanisms by allowing smaller clearances without yielding the beam material. The other portions of the suspension, including the contact surfaces and the shuttle, are straightforward to fabricate.

5.8 Recommendations for future research

One item of interest in future research is the use of tape springs as the rolling-contact beams. Tape springs have been investigated in previous work for their use in compliant mechanisms and have several unique characteristics that may be especially applicable in the RCC suspension. First, tape springs can be elastically deflected to a smaller radius than a flat leaf spring [20], resulting in a smaller clearance in the RCC suspension and thus a more compact mechanism. The individual tape spring beams also exhibit a stable position as a closed loop RCC beam, a position referred to by Vehar et al. as a two-fold loop [19]. Thus, a RCC beam made of a tape spring has zero restoring force at this point. Compressing the beam further would result in a restoring force with behavior somewhat similar the flat leaf spring RCC beam, although the force-deflection behavior has not been investigated at this time. The use of tape spring RCC beams with this stable position causes the individual force-deflection curves in Figure 5.9 to sharply decrease after a slight off-axis deflection. The increased net force results in higher off-axis stiffness.

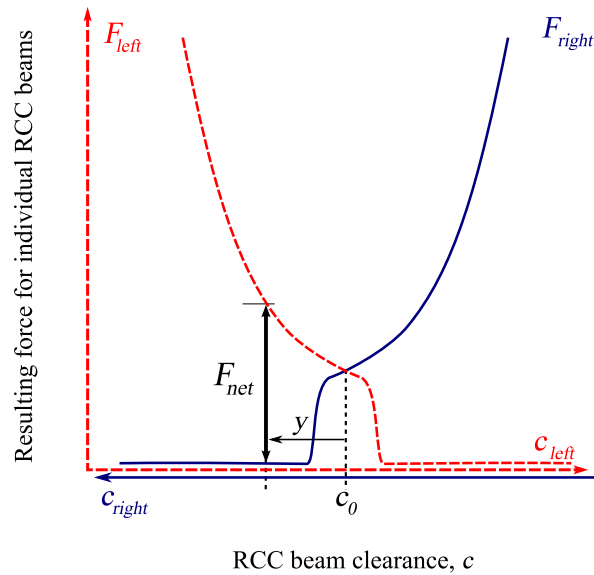


Figure 5.9: The use of tape springs in the RCC suspension could increase the stiffness because of the stable nature of the two-fold loop

Another variation in the RCC suspension that is an interest of future research would provide for the creation of stable positions using non-parallel contacting surfaces. As an example, consider an RCC suspension where the contacting surfaces have a depression where the radius of the beam can increase. The increased radius at this position will create a local minima in the potential energy stored in the beam, causing a stable position in the mechanism's travel. Other principles of stability could include variations in the beam geometry and contact surface protrusions. Theoretically it could be possible to create as many stable positions as are desired using these or other techniques [24].

5.9 Conclusions

This chapter has introduced a new configuration of linear mechanisms (the RCC suspension) and associated model that allows for very large displacements with consistent behavior. The benefits of the mechanism include both the consistently high off-axis stiffness compared to axial resistance and the frictionless rolling-contact motion. The suspension can operate independently or can also be superimposed onto other linear mechanisms to improve their off-axis stiffness.

Chapter 6

Conclusions

The overall objective of this thesis was to further the development of large-displacement linear-motion compliant mechanisms (LLCMs), with sub-objectives defined as: (1) develop an improved approach for evaluating the performance of large-displacement linear-motion compliant mechanisms; and (2) emerging from the principles found in the evaluation method, develop and present a new mechanism configuration that provides increased performance in linear motion, along with an associated design-oriented performance model for the new mechanism. In fulfillment of sub-objective (1), the metrics developed in Chapter 3 provide an improved approach for evaluating the performance of LLCMs, laying the groundwork for designers to develop mechanisms with improved performance. Sub-objective (2) is addressed in the description and development of the Rolling-Contact Compliant (RCC) suspension and the RCC beam pseudo-rigid-body model. The RCC suspension exhibits increased performance in linear motion, which is discussed in Chapter 5, with an associated design-oriented performance model for the new mechanism presented in Chapter 4. The following are some specific conclusions related to the sub-objectives of the thesis.

Chapter 3 has developed a foundation for the development and evaluation of new compliant linear mechanisms that can overcome the current displacement-stiffness trade-offs to yield much longer travel capabilities. The main outcomes of performance for LLCMs are enumerated in Chapter 3 as increased travel, increased transverse stiffness, increased torsional stiffness, decreased axial force, and decreased mechanism size. These are combined to formulate non-dimensional metrics, which can be used to evaluate mechanism designs. By applying the metrics to designs that span the design space of a given concept, the metrics create a performance region for the concept. This evaluation approach can be

used to compare the performance of different LLCM concepts. It was also shown that many previous linear mechanisms have low off-axis stiffness due to a decrease in off-axis stiffness when displaced from the home position. Therefore, the subsequent research focuses on a mechanism that exhibits consistent off-axis behavior for any position along the axis of travel.

In Chapter 4, the model for the RCC beam illustrates a number of desirable characteristics for this component with associated improvements in performance for the RCC suspension, including frictionless and neutrally-stable axial motion. Point-force loading at the point of contact allows the RCC beam to be represented by an equivalent pinned-pinned segment, identical to the curved segment of the RCC beam. The PRBM uses a half-model of the RCC beam, consisting of an initially straight cantilever beam loaded only in the horizontal direction. Equations for force and stress are developed in terms of the clearance between contact surfaces. This force-deflection equation is inversely proportional to the clearance between contact surfaces squared. Increasing yield strength quickly improves performance, allowing for higher forces and narrower clearances.

This work has also developed the techniques for modeling and comparing LLCMs and introduces a new configuration (the RCC suspension) and associated model that allows for very large displacements with consistent behavior. The benefits of the mechanism include both the consistently high off-axis stiffness compared to axial resistance and the frictionless rolling-contact motion. The suspension can operate independently or can also be superimposed onto other linear mechanisms to improve their off-axis stiffness.

Items of interest for future study of large-displacement linear-motion compliant mechanisms include:

- Extension of the performance metrics to out-of plane directions.
- Simulation and evaluation of a wide range of compliant linear-motion devices, including the exploration of bistable mechanisms, and subsequent development of performance regions for those devices. A survey of existing devices may elucidate features that create high performance in off-axis stiffness.

- Creation of multiple stable points along the axial travel with the RCC suspension. Potential strategies for creating stable positions include variations in beam properties and in wall geometry.
- Investigation of the RCC suspension using tape springs as RCC beams. Using tape springs may increase the net restoring force (and off-axis stiffness) and decrease the footprint by allowing a smaller radius.

References

- [1] Cannon, B. R., Lillian, T. D., Magleby, S. P., Howell, L. L., and Linford, M. R., 2005. “A compliant end-effector for microscribing.” *Precision engineering*, **29**, pp. 86–94.
- [2] Trease, B. P., Moon, Y.-M., and Kota, S., 2005. “Design of large-displacement compliant joints.” *Journal of Mechanical Design*, **127**, July, pp. 788–798.
- [3] Hubbard, N. B., Wittwer, J. W., Kennedy, J. A., Wilcox, D. L., and Howell, L. L., 2004. “A novel fully compliant planar linear-motion mechanism” *Proceedings of the ASME Design Engineering Technical Conference*, **2 A**, pp. 1 – 5.
- [4] Saggere, L., Kota, S., and Crary, S., 1994. “New design for suspension of linear microactuators.” *American Society of Mechanical Engineers, Dynamic Systems and Control Division (Publication) DSC*, **55-2**, pp. 671 – 675.
- [5] Gomm, T., Howell, L. L., and Selfridge, R., 2002. “In-plane linear displacement bistable microrelay.” *Journal of Micromechanics and Microengineering*, **12**, pp. 257–264.
- [6] Masters, N. D., and Howell, L. L., 2003. “A self-retracting fully compliant bistable micromechanism.” *Journal of Microelectromechanical Systems*, **12**(3), pp. 273 – 280. Fully compliant bistable micromechanisms;
- [7] Wilcox, D. L., and Howell, L. L., 2005. “Double-tensural bistable mechanisms (DTBM) with on-chip actuation and spring-like post-bistable behavior.” *Proceedings of the 2005 ASME Design Engineering Technical Conferences*.
- [8] Guerinot, A. E., Magleby, S. P., Howell, L. L., and Todd, R. H., 2005. “Compliant joint design principles for high compressive load situations.” *Journal of Mechanical Design*, **127**.
- [9] Leipholz, H. H. L., 1970. *Stability Theory : An introduction to the stability of dynamic systems and rigid bodies*. Academic press, San Diego, CA.
- [10] Jensen, B. D., and Howell, L. L., 2003. “Identification of compliant pseudo-rigid body mechanisms resulting in bistable behavior.” *Journal of Mechanical Design*, **125**(4), pp. 701–708.
- [11] Jensen, B. D., and Howell, L. L., 2004. “Bistable configurations of compliant mechanisms modeled using four links and translational joints.” *Journal of Mechanical Design*, **126**(4), pp. 657–666.

- [12] Howell, L., and Midha, A., 1995. “Parametric deflection approximations for end-loaded, large-deflection beams in compliant mechanisms.” *Journal of Mechanical Design, Transactions of the ASME*, **117**(1), pp. 156 – 165.
- [13] Edwards, B. J., Jensen, B. D., and Howell, L. L., 1999. “A pseudo-rigid-body model for functionally binary pinned-pinned segments used in compliant mechanisms.” *Proceedings of the 1999 ASME Design Engineering Technical Conferences*(DETC99/DAC-8644).
- [14] Howell, L. L., and Midha, A., 1996. “Parametric deflection approximations for initially curved, large-deflection beams in compliant mechanisms.” *Proceedings of the 1996 ASME Design Engineering Technical Conferences*(96-DETC/MECH-1215).
- [15] Howell, L. L., 2001. *Compliant Mechanisms*. John Wiley & Sons, New York.
- [16] Mankame, N. D., and Ananthasuresh, G. K., 2004. “A contact-aided compliant mechanical cycle doubler: Preliminary analysis and testing.” *Proceedings of the ASME Design Engineering Technical Conference*, **2**, pp. 1381–1388.
- [17] Mankame, N. D., and Ananthasuresh, G. K., 2004. “Topology optimization for synthesis of contact-aided compliant mechanisms.” *Computers and Structures*, **82**(15-16), June, pp. 1267–1290.
- [18] Cannon, J. R., and Howell, L. L., 2005. “A compliant contact-aided revolute joint.” *Mechanism and Machine Theory*, **40**, pp. 1273–1293.
- [19] Veihar, C., Kota, S., and Dennis, R., 2004. “Closed-loop tape springs as fully compliant mechanisms -preliminary investigations.” *Proceedings of the ASME Design Engineering Technical Conference*, **2 B**, pp. 1023 – 1032.
- [20] Seffen, K. A., 2001. “On the behavior of folded tape-springs.” *Transactions of the ASME. Journal of Applied Mechanics*, **68**(3), May, pp. 369–375.
- [21] Baker, M. S., Lyon, S. M., and Howell, L. L., 2000. “Design of FBPPs with the focal moment method.” *Proceedings of the 2000 ASME Design Engineering Technical Conferences*(DETC00/MECH-14117).
- [22] Wittwer, J. W., and Howell, L. L., 2002. “Design of a functionally binary pinned-pinned segment for use as a tension-compression spring in compliant micro mechanisms.” *American Society of Mechanical Engineers, Aerospace Division (Publication) AD*, **67**, pp. 197 – 204.
- [23] Cadman, R., 1970. Rolamite - Geometry and force analysis. Technical report, Sandia Laboratories, April.
- [24] Halverson, P. A., 2007. “Multi-stable compliant rolling-contact elements.” Master’s thesis, Brigham Young University.

Appendix A

Simulation of Sample Mechanisms

A.1 Folded Beam Simulation

The following batch file, written in the ANSYS Parametric Design Language (ADPL), generates data describing the axial and off-axis behavior along the length of travel for a single design of the Folded Beam [1]. Designs were simulated for polypropylene, with modulus of 1.138 GPa and yield strength of 34 Mpa, allowing the in-plane thickness of the flexures, denoted below as hf , to range from 1.25-3 mm.

```
!FOLDED BEAM MECHANISM
!Polypropylene Prototype
!Transverse Stiffness Analysis
!Developed by Neal Hubbard 31 Dec 2003
!Modified by Allen Mackay Jan 2007
/CLEAR,START
/TITLE,FOLDED BEAM MECHANISM
!=====
!Set input parameters.
!Unit System: mm, kg, s, mN, kPa
/PREP7
PI=3.1415926535
Ls=72 !Length of stiff shuttle segments
Lf=74.7 !Length of flexible segments
Lv=47.5 !Length of stiff vertical segments
hs=200 !In-plane thickness of stiff segments
hf=3.0 !In-plane thickness of flexible segments
bb=6.35 !Out-of-plane thickness of the model
Ex=1.138E6 !Young's Modulus
PRxy=0.3 !Poisson's Ratio

NELS=10 !Number of elements on Ls
NELF=25 !Number of elements on Lf
NELV=5 !Number of elements on Lv

ADmax=110 !Total axial displacement
TDmax=.1 !Total transverse displacement
RotMax=1*PI/360 !Total rotational displacement = 0.5 degrees
```

```

ADS=150 !Number of axial displacement steps
TDS=3 !Number of transverse displacement steps
!The total number of load steps will be NLS=(ADS+1)*(TDS+1).

```

```

!=====

```

```

!Define the element type and beam properties.

```

```

ET,1,BEAM3
R,1,bb*hs,bb*(hs**3)/12,hs,1.2,0,0
R,2,bb*hf,bb*(hf**3)/12,hf,1.2,0,0
MP,EX,1,Ex
MP,GXY,1,Ex/(2*(1+PRxy))

```

```

!Place key points.

```

```

K,1,0,0
K,2,Ls,0
K,3,2*Ls,0
K,4,3*Ls,0
K,5,0,Lv
K,6,Ls,Lv
K,7,2*Ls,Lv
K,8,3*Ls,Lv
K,9,0,Lv+Lf
K,10,Ls,Lv+Lf
K,11,2*Ls,Lv+Lf
K,12,3*Ls,Lv+Lf
K,13,0,-Lv
K,14,Ls,-Lv
K,15,2*Ls,-Lv
K,16,3*Ls,-Lv
K,17,0,-Lv-Lf
K,18,Ls,-Lv-Lf
K,19,2*Ls,-Lv-Lf
K,20,3*Ls,-Lv-Lf

```

```

!Draw lines.

```

```

L,1,2,NELS !Line 1
L,2,3,NELS !Line 2
L,3,4,NELS !Line 3
L,1,5,NELV !Line 4
L,1,13,NELV !Line 5
L,4,8,NELV !Line 6
L,4,16,NELV !Line 7
L,5,9,NELF !Line 8
L,6,10,NELF !Line 9

```

```
L,7,11,NELF !Line 10
L,8,12,NELF !Line 11
L,13,17,NELF !Line 12
L,14,18,NELF !Line 13
L,15,19,NELF !Line 14
L,16,20,NELF !Line 15
L,9,10,NELS !Line 16
L,10,11,NELS !Line 17
L,11,12,NELS !Line 18
L,17,18,NELS !Line 19
L,18,19,NELS !Line 20
L,19,20,NELS !Line 21
```

```
!Mesh the lines with beam elements.
```

```
TYPE,1
MAT,1
REAL,1
LMESH,1,7,1
LMESH,16,21,1
```

```
REAL,2
LMESH,8,15,1
/SHRINK,.5
```

```
!Find the node number of the key point at left end of the shuttle.
```

```
KSEL,S,KP,,1
NSLK,S
*get,nleft,NODE,0,NUM,MAX
NSEL,ALL
KSEL,ALL
```

```
!Find the node number of the key point at center of the shuttle.
```

```
KSEL,S,KP,,3
NSLK,S
*get,nctr,NODE,0,NUM,MAX
NSEL,ALL
KSEL,ALL
```

```
!Find the node number of the key point at right end of the shuttle.
```

```
KSEL,S,KP,,4
NSLK,S
*get,nright,NODE,0,NUM,MAX
NSEL,ALL
KSEL,ALL
FINISH
```



```

!=====
!Solve the model.
/SOLU
!(ANTYPE, Analysis type, Status [NEW or REST], Load step for a
!multiframe restart, Substep, Action)
ANTYPE,STATIC, , ,
!(SOLCONTROL, Optimized defaults, Check contact state, Pressure load
!stiffness, Volumetric compatibility tolerance)
SOLCONTROL,ON, , ,
!(NLGEOM, Large deformation effects) Stress stiffening is also active.
NLGEOM,ON
!(NROPT, Newton-Raphson option, Unused, Adaptive descent key)
NROPT,FULL, ,OFF
!(NSUBST, Size of the first substep in each load step, Maximum number
!of substeps, Minimum number, Carry-over key)
NSUBST,1,10,1,OFF
!(AUTOTS, Automatic time stepping)
AUTOTS,ON
!(CNVTOL, Label, Convergence value, Tolerance about value, Norm,
!Minimum for the program-calculated reference value)
CNVTOL,F, .0001, .1
CNVTOL,U, .0001, .1

!Apply constraints
DK,6,ALL,0
DK,7,ALL,0
DK,14,ALL,0
DK,15,ALL,0

!Apply incremental displacements to the center shuttle.
j=0 !Load step index
*DO,mm,0,ADS
  DK,1,UX,mm*ADmax/ADS
  DK,1,UY,0
  DK,4,UY,0
  j=j+1
  LSWRITE,j

!Apply Rotational Displacement (remove translational displacement)
  DKDELE,1, UY
  DKDELE,4, UY
  DK,1, ROTZ,RotMax
  j=j+1
  LSWRITE,j

```

```

!Apply Transverse Displacement (remove rotational displacement)
  DKDELE,1, ROTZ
  *DO,nn,1,TDS
  DK,1,UY,nn*TDmax/TDS
  DK,4,UY,nn*TDmax/TDS
  j=j+1
  LSWRITE,j
  *ENDDO
*ENDDO

LSSOLVE,1,j
FINISH

!-----
!Compile results.
/POST1
!(*DIM, Name of array, array type, # rows, # columns, # planes,
!Names of index vectors)
*DIM,ADsp, ,j
*DIM,TDsp, ,j
*DIM,TDspC, ,j
*DIM,AFr, ,j
*DIM,TFr, ,j
*DIM,Smax, ,j
*DIM,RotDisp, ,j
*DIM,Torq, ,j

!(ETABLE, Label for table, Item, Component)
ETABLE,smxi,NMIS,1
ETABLE,smxj,NMIS,3
ETABLE,smni,NMIS,2
ETABLE,smnj,NMIS,4

*DO,i,1,j
!(SET, Load step, Substep, Scale factor, Complex component, Time,
!Angle, Data set number)
SET,i
ADsp(i)=UX(nleft)
TDsp(i)=UY(nleft)
TDspC(i)=UY(nctr)
RotDisp(i)=ROTZ(nleft)
!(*GET, Variable, Entity, Entity number, Item name, Item label)
*GET,value,NODE,nleft,RF,FX
AFr(i)=value

```

```

*GET,Fleft,NODE,nleft,RF,FY
*GET,Fright,NODE,nright,RF,FY
TFr(i)=Fleft+Fright
*GET,torque,NODE,nleft,RF,ROTZ
Torq(i)=torque

ETABLE,REFL
!(ESORT, ETAB, Element table, Accending order, Absolute value, Number
!of elements)
ESORT,ETAB,smxi,0,0
*GET,maxi,SORT,0,MAX
ESORT,ETAB,smxj,0,0
*GET,maxj,SORT,0,MAX
ESORT,ETAB,smni,0,0
*GET,mini,SORT,0,MIN
ESORT,ETAB,smnj,0,0
*GET,minj,SORT,0,MIN
Smax(i)=MAX(maxi,maxj,-mini,-minj)
*ENDDO

!Output results to a file.
!(/OUTPUT, Filename, Extension, Directory, Location in file)
/OUTPUT,FB_Results.txt
*MSG,INFO,'Step','Ax Disp','Tr Disp','Tr Disp Ctr','Ax Force',
'Tr Force','Max Stress'
%-4C %-12C %-12C %-12C %-12C %-12C %-12C
*VWRITE,SEQU,ADsp(1),TDsp(1),TDspC(1),AFr(1),TFr(1),
Smax(1),RotDisp(1),Torq(1)
%3I %-12.4G %-12.4G %-12.4G %-12.4G %-12.4G
%-12.3G%-12.5G%-12.4G
/OUTPUT

!PLDISP,1
PLETAB,smxi,NOAV
FINISH

```

A.2 CT Joint Simulation

The following batch file, written in the ANSYS Parametric Design Language (ADPL), generates data describing the axial and off-axis behavior along the length of travel for a single design of the CT joint [2]. Designs were simulated for polypropylene, with modulus of 1.138 GPa and yield strength of 34 Mpa, allowing the in-plane thickness of the flexures, denoted below as $h1$, to range from 1.25-3 mm.

```
/CLEAR,START
```

```
/TITLE,CT Joint: A Linear Suspension Developed by Trease, et al.  
!Developed by Neal Hubbard Dec 2003  
!Modified by Allen Mackay Jan 2007
```

```
!Polypropylene Prototype
```

```
/PREP7
```

```
!-----PARAMETERS-----
```

```
!Unit System: mm, kg, s, mN, kPa
```

```
PI=acos(-1.)
```

```
Ex=1.138E6 !Young's Modulus
```

```
PRxy=.3 !Poisson's Ratio
```

```
!Design Parameters
```

```
Lf = 80 ! Length of Flexible Segments
```

```
Ls = 10 ! Length of Stiff segments
```

```
base=6.35 !Thickness of mechanism
```

```
h1=3.0 !Height (cubed dim) of flexible segments
```

```
h2=100 !Height (cubed dim) of stiff segments
```

```
!Model Parameters
```

```
ADmax=110 !Total axial displacement
```

```
TDmax=0.7 !Total transverse displacement
```

```
RotMax=1*PI/360 !Total rotational displacement = 0.5 degrees
```

```
SegCompliant=25 !Number of elements in flexible segments
```

```
SegStiff=5 !Number of elements in stiff segments
```

```
ADS=190 !Axial displacement steps
```

```
TDS=3 !Transverse displacement steps
```

```
!The total number of load steps will be NLS=(ADS+1)*(TDS+1).
```

```
!-----DEFINE GEOMETRY-----
```

```
K,1,0,0
```

```
K,2,0,-Lf
```

```
K,3,0,Lf
```

```
K,4,Ls,0
```

```
K,5,Ls,-Lf
```

```
K,6,Ls,Lf
```

```
K,7,2*Ls, 0
```

```
K,8,2*Ls, -Lf
```

```
K,9,2*Ls, Lf
```

```
K,10,3*Ls,0
```

```
K,11,3*Ls,-Lf
```

```
K,12,3*Ls,Lf
```

! Second Half of mechanism

K,13,7* L_s ,0
K,14,7* L_s ,-Lf
K,15,7* L_s ,Lf
K,16,8* L_s , 0
K,17,8* L_s , -Lf
K,18,8* L_s , Lf
K,19,9* L_s , 0
K,20,9* L_s , -Lf
K,21,9* L_s , Lf
K,22,10* L_s ,0
K,23,10* L_s , -Lf
K,24,10* L_s ,Lf

!Create Line

L,1,2
L,1,3
L,1,4
L,2,5
L,3,6
L,4,5
L,4,6
L,4,7
L,5,8
L,6,9
L,7,8
L,7,9
L,7,10
L,8,11
L,9,12
L,10,11
L,10,12
L,11,14
L,12,15

!Second Half of mechanisms

L,13,14
L,13,15
L,13,16
L,14,17
L,15,18
L,16,17
L,16,18
L,16,19
L,17,20

L,18,21
L,19,20
L,19,21
L,19,22
L,20,23
L,21,24
L,22,23
L,22,24

LESIZE,1,,SegCompliant
LESIZE,2,,SegCompliant
LESIZE,3,,SegStiff
LESIZE,4,,SegStiff
LESIZE,5,,SegStiff
LESIZE,6,,SegCompliant
LESIZE,7,,SegCompliant
LESIZE,8,,SegStiff
LESIZE,9,,SegStiff
LESIZE,10,,SegStiff
LESIZE,11,,SegCompliant
LESIZE,12,,SegCompliant
LESIZE,13,,SegStiff
LESIZE,14,,SegStiff
LESIZE,15,,SegStiff
LESIZE,16,,SegCompliant
LESIZE,17,,SegCompliant
LESIZE,18,,SegStiff
LESIZE,19,,SegStiff

! Second Half of Mechanism
LESIZE,20,,SegCompliant
LESIZE,21,,SegCompliant
LESIZE,22,,SegStiff
LESIZE,23,,SegStiff
LESIZE,24,,SegStiff
LESIZE,25,,SegCompliant
LESIZE,26,,SegCompliant LESIZE,27,,SegStiff
LESIZE,28,,SegStiff
LESIZE,29,,SegStiff
LESIZE,30,,SegCompliant
LESIZE,31,,SegCompliant
LESIZE,32,,SegStiff
LESIZE,33,,SegStiff
LESIZE,34,,SegStiff

```

LESIZE,35,,SegCompliant
LESIZE,36,,SegCompliant

! Fit to Screen
/AUTO,1

! Set deflection to 1:1 scale
/DSCALE,1,1

! Command to Display Lines: L PLOT, Nodes: N PLOT, Key: K PLOT,ALL
L PLOT
K PLOT,ALL

!-----CREATE MESH-----
ET,1,BEAM3

!Area Properties
Iz1 = base*h1*h1*h1/12 !Moment of inertia for flexible members
Iz2 = base*h2*h2*h2/12 !Moment of inertia for stiff members
Acr1 = base*h1 !Cross sectional area of flexible members
Acr2 = base*h2 !Cross sectional area of stiff members

R,1,Acr1,Iz1,h1,1.2,0,0 !Flexible segments
R,2,Acr2,Iz2,h2,1.2,0,0 !Stiff segments

MP,EX,1,Ex
MP,GXY,1,Ex/(2*(1+PRxy))
MP,REFT,1,0

!Flexible Segments
REAL,1
TYPE,1
MAT,1
LMESH,1
LMESH,2
LMESH,6
LMESH,7
LMESH,11
LMESH,12
LMESH,16
LMESH,17
! Second Half of Mechanism
LMESH,20
LMESH,21

```

```
LMESH,25
LMESH,26
LMESH,30
LMESH,31
LMESH,35
LMESH,36
```

```
REAL,2
LMESH,3,5,1
LMESH,8,10,1
LMESH,13,15,1
LMESH,18,19,1
! Second Half of Mechanism
LMESH,22,24,1
LMESH,27,29,1
LMESH,32,34,1
```

```
KSEL,S,KP,,1 !Selects key point 1
NSLK,S !Finds nodes assoc with sel KP
*GET,nleft,NODE,0,NUM,MAX !Stores node number at left end of shuttle
NSEL,ALL !Reselects all nodes for subsequent analysis
KSEL,ALL !Turns KP back on; allows selection of other KP
```

```
KSEL,S,KP,,10 !Selects key point 10
NSLK,S !Finds nodes assoc with sel KP
*GET,nleftctr,NODE,0,NUM,MAX !Stores node number at center of shuttle
NSEL,ALL !Reselects all nodes for subsequent analysis
KSEL,ALL !Turns KP back on; allows selection of other KP
```

```
KSEL,S,KP,,13 !Selects key point 13
NSLK,S !Finds nodes assoc with sel KP
*GET,nrightctr,NODE,0,NUM,MAX !node number at right end of shuttle
NSEL,ALL !Reselects all nodes for subsequent analysis
KSEL,ALL !Turns KP back on; allows selection of other KP
```

```
KSEL,S,KP,,22 !Selects key point 22
NSLK,S !Finds nodes assoc with sel KP
*GET,nright,NODE,0,NUM,MAX !Stores node number at right end of shuttle
NSEL,ALL !Reselects all nodes for subsequent analysis
KSEL,ALL !Turns KP back on; allows selection of other KP
```

```
FINISH
```



```

!-----SOLVE-----
/SOLU
!(ANTYPE, Analysis type, Status [NEW or REST], Load step for a
!multiframe restart, Substep, Action)
ANTYPE,STATIC, , ,
!(SOLCONTROL, Optimized defaults, Check contact state, Pressure load
!stiffness, Volumetric compatibility tolerance)
SOLCONTROL,ON, , ,
!(NLGEOM, Large deformation effects) Stess stiffening is also active.
NLGEOM,ON
!(NROPT, Newton-Raphson option, Unused, Adaptive descent key)
NROPT,FULL, ,OFF
!(NSUBST, Size of the first substep in each load step, Maximum number
!of substeps, Minimum number, Carry-over key)
NSUBST,1,10,1,OFF
!(AUTOTS, Automatic time stepping)
AUTOTS,ON
!(CNVTOL, Label, Convergence value, Tolerance about value, Norm,
!Minimum for the program-calculated reference value)
CNVTOL,F, ,.0001, ,.1
CNVTOL,U, ,.0001, ,.1

!Fixed end constraints
DK,1, ,0, , , ,UX,UY , , ,
DK,10, ,0, , , ,UY, , , , ,

!Apply displacements
j=0 !Load step index
*DO,mm,0,ADS
!Apply axial displacement
DK,13,UX,mm*ADmax/ADS
DK,13, UY,0
DK,22, UY,0
j=j+1
LSWRITE,j

!Apply Rotational Displacement (and remove translational displacement)
DKDELE,13, UY
DKDELE,22, UY
DK,13, ROTZ, RotMax
j=j+1
LSWRITE,j

!Apply Transverse Displacement (and remove rotational displacment)
DKDELE,13, ROTZ

```

```

        *DO,nn,1,TDS
        DK,13,UY,nn*TDmax/TDS
        DK,22,UY,nn*TDmax/TDS
        j=j+1
        LSWRITE,j
    *ENDDO
*ENDDO

LSSOLVE,1,j
FINISH

!-----COMPILE AND REPORT RESULTS-----
/POST1
!(*DIM, Name of array, array type, # rows, # columns, # planes, Names
!of index vectors)
*DIM,ADsp, ,j
*DIM,TDsp, ,j
*DIM,TDspC, ,j
*DIM,AFr, ,j
*DIM,TFr, ,j
*DIM,Smax, ,j
*DIM,RotDisp, ,j
*DIM,Torq, ,j

!SET, LAST
ETABLE,smxi,NMIS,1
ETABLE,smxj,NMIS,3
ETABLE,smni,NMIS,2
ETABLE,smnj,NMIS,4

*DO,i,1,j
!(SET, Load step, Substep, Scale factor, Complex component, Time,
!Angle, Data set number)
SET,i
ADsp(i)=UX(nrightctr)
TDsp(i)=UY(nrightctr)
TDspC(i)=UY(nright)
RotDisp(i)=ROTZ(nrightctr)
!(*GET, Variable, Entity, Entity number, Item name, Item label)
*GET,value,NODE,nleft,RF,FX
AFr(i)=-value
*GET,Fleft,NODE,nleft,RF,FY
*GET,Fleftctr,NODE,nleftctr,RF,FY
TFr(i)=-Fleft-Fleftctr
*GET,valueT,NODE,nrightctr,RF,MZ

```

```

Torq(i)=valueT

ETABLE,REFL
!(ESORT, ETAB, Element table, Accending order, Absolute value, Number
!of elements)
ESORT,ETAB,smxi,0,0
*GET,maxi,SORT,0,MAX
ESORT,ETAB,smxj,0,0
*GET,maxj,SORT,0,MAX
ESORT,ETAB,smni,0,0
*GET,mini,SORT,0,MIN
ESORT,ETAB,smnj,0,0
*GET,minj,SORT,0,MIN
Smax(i)=MAX(maxi,maxj,-mini,-minj)
*ENDDO

!Output results to a file.
!(/OUTPUT, Filename, Extension, Directory, Location in file)
/OUTPUT,CT_Results,txt
*MSG,INFO,'Step','AxDisp','TrDisp','TrDispCtr','AxForce',
'TrForce','MaxStress','RotDisp','Torq(1)'
%-4C %-12C %-12C %-12C %-12C %-12C %-12C
*VWRITE,SEQU,ADsp(1),TDsp(1),TDspC(1),AFr(1),TFr(1),
Smax(1), RotDisp(1),Torq(1)
%3I %-12.4G %-12.4G %-12.4G %-12.4G %-12.4G
%-12.3G%-12.5G%-12.4G
/OUTPUT

!PLDISP,1
PLETAB,smxi,NOAV
FINISH

```

A.3 XBob Simulation

The following batch file, written in the ANSYS Parametric Design Language (APDL), generates data describing the axial and off-axis behavior along the length of travel for a single design of the XBob [3]. Designs were simulated for polypropylene, with modulus of 1.138 GPa and yield strength of 34 Mpa, allowing the in-plane thickness of the flexures, denoted below as h_1 , to range from 1.25-2.5 mm.

```

/CLEAR,START
/TITLE,XBOB: A Linear Suspension Based on the Roberts Mechanism
!Developed by Neal Hubbard Dec 2003
!Modified by Allen Mackay Jan 2007

```

```

!Polypropylene Prototype
/PREP7

!-----PARAMETERS-----
!Unit System: mm, kg, s, mN, kPa
PI=acos(-1.)
Ex=1.138E6 !Young's Modulus
PRxy=.3 !Poisson's Ratio

!Design Parameters
thetad=70 !Angle of flexible segments (degrees)
theta =thetad*PI/180 !Angle of flexible segments (radians)
Lco=75 !Length of outer flexible segments
Lci=Lco !Length of inner flexible segments
Lm=44.53 !Length of beams at each end of rotating beams
Lr=171.39 !Length of rotating beams
La=106 !Length of vertical beams attached to shuttle
Ls1=95.833 !Length of shuttle for half of mechanism
Ls2=25 !Length of shuttle extension joining two halves

base=6.35 !Thickness of mechanism
h1=2.5 !Height (cubed dim) of flexible segments
h2=25 !Height (cubed dim) of stiff segments

!Model Parameters
ADmax=110 !Total axial displacement
TDmax=0.7 !Total transverse displacement
RotMax = 1*PI/360 !Total rotational displacement = 0.5 degrees

SegCompliant=25 !Number of elements in flexible segments
SegStiff=5 !Number of elements in stiff segments
ADS=190 !Axial displacement steps
TDS=3 !Transverse displacement steps
!The total number of load steps will be NLS=(ADS+1)*(TDS+1).

!-----DEFINE GEOMETRY-----
K,1,(Lci-Lco)*cos(theta),La-(Lci+Lco)*sin(theta)+Lr,0
K,2,Lci*cos(theta),La+Lr-Lci*sin(theta),0
K,3,Lm+Lci*cos(theta),La+Lr-Lci*sin(theta),0
K,4,Lm+(Lci+Lco)*cos(theta),La-(Lci+Lco)*sin(theta)+Lr,0
K,5,Lci*cos(theta)+Lm/2,La+Lr-Lci*sin(theta),0
K,6,Lci*cos(theta)+Lm/2,La-Lci*sin(theta),0
K,7,0,La,0
K,8,Lci*cos(theta),La-Lci*sin(theta),0
K,9,Lci*cos(theta)+Lm,La-Lci*sin(theta),0

```

K,10,Ls1,La,0
 K,11,0,0,0
 K,12,Ls1,0,0
 K,13,Ls1+Ls2,0,0
 K,14,0,-La,0
 K,15,Lci*cos(theta),-(La-Lci*sin(theta)),0
 K,16,Lci*cos(theta)+Lm,-(La-Lci*sin(theta)),0
 K,17,Ls1,-La,0
 K,18,Lci*cos(theta)+Lm/2,-(La-Lci*sin(theta)),0
 K,19,Lci*cos(theta)+Lm/2,-(La+Lr-Lci*sin(theta)),0
 K,20,(Lci-Lco)*cos(theta),-(La-(Lci+Lco)*sin(theta)+Lr),0
 K,21,Lci*cos(theta),-(La+Lr-Lci*sin(theta)),0
 K,22,Lm+Lci*cos(theta),-(La+Lr-Lci*sin(theta)),0
 K,23,Lm+(Lci+Lco)*cos(theta),-(La-(Lci+Lco)*sin(theta)+Lr),0
 ! Second Half of mechanism
 K,24,Ls1+Ls2+(Lci-Lco)*cos(theta),La-(Lci+Lco)*sin(theta)+Lr,0
 K,25,Ls1+Ls2+Lci*cos(theta),La+Lr-Lci*sin(theta),0
 K,26,Ls1+Ls2+Lm+Lci*cos(theta),La+Lr-Lci*sin(theta),0
 K,27,Ls1+Ls2+Lm+(Lci+Lco)*cos(theta),La-(Lci+Lco)*sin(theta)+Lr,0
 K,28,Ls1+Ls2+Lci*cos(theta)+Lm/2,La+Lr-Lci*sin(theta),0
 K,29,Ls1+Ls2+Lci*cos(theta)+Lm/2,La-Lci*sin(theta),0
 K,30,Ls1+Ls2+0,La,0
 K,31,Ls1+Ls2+Lci*cos(theta),La-Lci*sin(theta),0
 K,32,Ls1+Ls2+Lci*cos(theta)+Lm,La-Lci*sin(theta),0
 K,33,Ls1+Ls2+Ls1,La,0
 K,35,Ls1+Ls2+Ls1,0,0
 K,36,Ls1+Ls2+0,-La,0
 K,37,Ls1+Ls2+Lci*cos(theta),-(La-Lci*sin(theta)),0
 K,38,Ls1+Ls2+Lci*cos(theta)+Lm,-(La-Lci*sin(theta)),0
 K,39,Ls1+Ls2+Ls1,-La,0
 K,40,Ls1+Ls2+Lci*cos(theta)+Lm/2,-(La-Lci*sin(theta)),0
 K,41,Ls1+Ls2+Lci*cos(theta)+Lm/2,-(La+Lr-Lci*sin(theta)),0
 K,42,Ls1+Ls2+(Lci-Lco)*cos(theta),-(La-(Lci+Lco)*sin(theta)+Lr),0
 K,43,Ls1+Ls2+Lci*cos(theta),-(La+Lr-Lci*sin(theta)),0
 K,44,Ls1+Ls2+Lm+Lci*cos(theta),-(La+Lr-Lci*sin(theta)),0
 K,45,Ls1+Ls2+Lm+(Lci+Lco)*cos(theta),-(La-(Lci+Lco)*sin(theta)+Lr),0

 L,1,2 ! Line 1
 L,2,5 ! Line 2
 L,5,3 ! Line 3
 L,3,4 ! Line 4
 L,5,6 ! Line 5
 L,7,8 ! Line 6
 L,8,6 ! Line 7
 L,6,9 ! Line 8

L,9,10 ! Line 9
L,7,11 ! Line 10
L,10,12 ! Line 11
L,11,12 ! Line 12
L,12,13 ! Line 13
L,11,14 ! Line 14
L,12,17 ! Line 15
L,14,15 ! Line 16
L,15,18 ! Line 17
L,18,16 ! Line 18
L,16,17 ! Line 19
L,18,19 ! Line 20
L,20,21 ! Line 21
L,21,19 ! Line 22
L,19,22 ! Line 23
L,22,23 ! Line 24
! Second Half of Mechanism
L,24,25 ! Line 25
L,25,28 ! Line 26
L,28,26 ! Line 27
L,26,27 ! Line 28
L,28,29 ! Line 29
L,30,31 ! Line 30
L,31,29 ! Line 31
L,29,32 ! Line 32
L,32,33 ! Line 33
L,30,13 ! Line 34
L,33,35 ! Line 35
L,13,35 ! Line 36
L,13,36 ! Line 37
L,35,39 ! Line 38
L,36,37 ! Line 39
L,37,40 ! Line 40
L,40,38 ! Line 41
L,38,39 ! Line 42
L,40,41 ! Line 43
L,42,43 ! Line 44
L,43,41 ! Line 45
L,41,44 ! Line 46
L,44,45 ! Line 47

LESIZE,1,,SegCompliant
LESIZE,2,,SegStiff
LESIZE,3,,SegStiff
LESIZE,4,,SegCompliant

LESIZE,5,,SegStiff
LESIZE,6,,SegCompliant
LESIZE,7,,SegStiff
LESIZE,8,,SegStiff
LESIZE,9,,SegCompliant
LESIZE,10,,SegStiff
LESIZE,11,,SegStiff
LESIZE,12,,SegStiff
LESIZE,13,,SegStiff
LESIZE,14,,SegStiff
LESIZE,15,,SegStiff
LESIZE,16,,SegCompliant
LESIZE,17,,SegStiff
LESIZE,18,,SegStiff
LESIZE,19,,SegCompliant
LESIZE,20,,SegStiff
LESIZE,21,,SegCompliant
LESIZE,22,,SegStiff
LESIZE,23,,SegStiff
LESIZE,24,,SegCompliant
! Second Half of Mechanism
LESIZE,25,,SegCompliant
LESIZE,26,,SegStiff
LESIZE,27,,SegStiff
LESIZE,28,,SegCompliant
LESIZE,29,,SegStiff
LESIZE,30,,SegCompliant
LESIZE,31,,SegStiff
LESIZE,32,,SegStiff
LESIZE,33,,SegCompliant
LESIZE,34,,SegStiff
LESIZE,35,,SegStiff
LESIZE,36,,SegStiff
LESIZE,37,,SegStiff
LESIZE,38,,SegStiff
LESIZE,39,,SegCompliant
LESIZE,40,,SegStiff
LESIZE,41,,SegStiff
LESIZE,42,,SegCompliant
LESIZE,43,,SegStiff
LESIZE,44,,SegCompliant
LESIZE,45,,SegStiff
LESIZE,46,,SegStiff
LESIZE,47,,SegCompliant

```

! Fit to Screen
/AUTO,1

! Set deflection to 1:1 scale
/DSCALE,1,1

! Command to Display Lines: L PLOT, Nodes: N PLOT, Key: K PLOT,ALL
L PLOT
K PLOT,ALL

!-----CREATE MESH-----
ET,1,BEAM3

!Area Properties
Iz1 = base*h1*h1*h1/12 !Moment of inertia for flexible members
Iz2 = base*h2*h2*h2/12 !Moment of inertia for stiff members
Acr1 = base*h1 !Cross sectional area of flexible members
Acr2 = base*h2 !Cross sectional area of stiff members

R,1,Acr1,Iz1,h1,1.2,0,0 !Flexible segments
R,2,Acr2,Iz2,h2,1.2,0,0 !Stiff segments

MP,EX,1,Ex
MP,GXY,1,Ex/(2*(1+PRxy))
MP,REFT,1,0

REAL,1
TYPE,1
MAT,1
LMESH,1
LMESH,4
LMESH,6
LMESH,9
LMESH,16
LMESH,19
LMESH,21
LMESH,24
! Second Half of Mechanism
LMESH,25
LMESH,28
LMESH,30
LMESH,33
LMESH,39
LMESH,42
LMESH,44

```



```

LMESH,47

REAL,2
LMESH,2,3,1
LMESH,5
LMESH,7,8
LMESH,10,15,1
LMESH,17,18,1
LMESH,20
LMESH,22,23,1
! Second Half of Mechanism
LMESH,26,27,1
LMESH,29
LMESH,31,32
LMESH,34,38,1
LMESH,40,41,1
LMESH,43
LMESH,45,46,1

KSEL,S,KP,,11 !Selects key point 11
NSLK,S !Finds nodes assoc with sel KP
*GET,nleft,NODE,0,NUM,MAX !Stores node number at left end of shuttle
NSEL,ALL !Reselects all nodes for subsequent analysis
KSEL,ALL !Turns KP back on; allows selection of other KP

KSEL,S,KP,,13 !Selects key point 13
NSLK,S !Finds nodes assoc with sel KP
*GET,nctr,NODE,0,NUM,MAX !Stores node number at center of shuttle
NSEL,ALL !Reselects all nodes for subsequent analysis
KSEL,ALL !Turns KP back on; allows selection of other KP

KSEL,S,KP,,35 !Selects key point 35
NSLK,S !Finds nodes assoc with sel KP
*GET,nright,NODE,0,NUM,MAX !Stores node number at right end of shuttle
NSEL,ALL !Reselects all nodes for subsequent analysis
KSEL,ALL !Turns KP back on; allows selection of other KP
FINISH

!-----SOLVE-----
/SOLU
!(ANTYPE, Analysis type, Status [NEW or REST], Load step for a
!multiframe restart, Substep, Action)
ANTYPE,STATIC, , ,
!(SOLCONTROL, Optimized defaults, Check contact state, Pressure load
!stiffness, Volumetric compatibility tolerance)

```

```

SOLCONTROL,ON, , ,
!(NLGEOM, Large deformation effects) Stess stiffening is also active.
NLGEOM,ON
!(NROPT, Newton-Raphson option, Unused, Adaptive descent key)
NROPT,FULL, ,OFF
!(NSUBST, Size of the first substep in each load step, Maximum number
!of substeps, Minimum number, Carry-over key)
NSUBST,1,10,1,OFF
!(AUTOTS, Automatic time stepping)
AUTOTS,ON
!(CNVTOL, Label, Convergence value, Tolerance about value, Norm,
!Minimum for the program-calculated reference value)
CNVTOL,F, ,.0001, ,.1
CNVTOL,U, ,.0001, ,.1

!Fixed end constraints
DK,1, ,0, , , ,UX,UY,ROTZ, , , ,
DK,4, ,0, , , ,UX,UY,ROTZ, , , ,
DK,20, ,0, , , ,UX,UY,ROTZ, , , ,
DK,23, ,0, , , ,UX,UY,ROTZ, , , ,
DK,24, ,0, , , ,UX,UY,ROTZ, , , ,
DK,27, ,0, , , ,UX,UY,ROTZ, , , ,
DK,42, ,0, , , ,UX,UY,ROTZ, , , ,
DK,45, ,0, , , ,UX,UY,ROTZ, , , ,

!Apply displacements
j=0 !Load step index
*DO,mm,0,ADS
  DK,11,UX,mm*ADmax/ADS
  DK,11,UY,0
  DK,35,UY,0
  j=j+1
  LSWRITE,j

!Apply Rotational Displacement (and remove translational displacement)
  DKDELE,11, UY
  DKDELE,35, UY
  DK,11, ROTZ, RotMax
  j=j+1
  LSWRITE,j

!Apply Transverse Displacement (and remove rotational displacment)
  DKDELE,11, ROTZ
  *DO,nn,1,TDS
  DK,11,UY,nn*TDmax/TDS

```

```

        DK,35,UY,nn*TDmax/TDS
        j=j+1
        LSWRITE,j
    *ENDDO
*ENDDO

LSSOLVE,1,j
FINISH

!-----COMPILE AND REPORT RESULTS-----
/POST1
!(*DIM, Name of array, array type, # rows, # columns, # planes, Names
!of index vectors)
*DIM,ADsp, ,j
*DIM,TDsp, ,j
*DIM,TDspC, ,j
*DIM,AFr, ,j
*DIM,TFr, ,j
*DIM,Smax, ,j
*DIM,RotDisp, ,j
*DIM,Torq, ,j

!SET, LAST
ETABLE,smxi,NMIS,1
ETABLE,smxj,NMIS,3
ETABLE,smni,NMIS,2
ETABLE,smnj,NMIS,4

*DO,i,1,j
!(SET, Load step, Substep, Scale factor, Complex component, Time,
!Angle, Data set number)
SET,i
ADsp(i)=UX(nleft)
TDsp(i)=UY(nleft)
TDspC(i)=UY(nctr)
RotDisp(i)=ROTZ(nleft)

!(*GET, Variable, Entity, Entity number, Item name, Item label)
*GET,value,NODE,nleft,RF,FX
AFr(i)=value
*GET,Fleft,NODE,nleft,RF,FY
*GET,Fright,NODE,nright,RF,FY
TFr(i)=Fleft+Fright
*GET,valueT,NODE,nleft,RF,MZ
Torq(i)=valueT

```

```

ETABLE,REFL
!(ESORT, ETAB, Element table, Accending order, Absolute value, Number
!of elements)
ESORT,ETAB,smxi,0,0
*GET,maxi,SORT,0,MAX
ESORT,ETAB,smxj,0,0
*GET,maxj,SORT,0,MAX
ESORT,ETAB,smni,0,0
*GET,mini,SORT,0,MIN
ESORT,ETAB,smnj,0,0
*GET,minj,SORT,0,MIN
Smax(i)=MAX(maxi,maxj,-mini,-minj)
*ENDDO

!Output results to a file.
!(/OUTPUT, Filename, Extension, Directory, Location in file)
/OUTPUT,XBob_Results.txt
*MSG,INFO,'Step','AxDisp','TrDisp','TrDispCtr','AxForce',
'TrForce','MaxStress'
%-4C %-12C %-12C %-12C %-12C %-12C %-12C
*VWRITE,SEQU,ADsp(1),TDsp(1),TDspC(1),AFr(1),TFr(1),
Smax(1), RotDisp(1),Torq(1)
%3I %-12.4G %-12.4G %-12.4G %-12.4G %-12.4G
%-12.3G%-12.5G%-12.4G
/OUTPUT

!PLDISP,1
PLETAB,smxi,NOAV
FINISH

```